Title

Coupled Transport Processes in Semipermeable Media. II: Numerical Method and Results

Authors

Jacobsen, J.S.
Carnahan, C.L.

Publication Date

1990-04-01

LBL-25619
UC-403

Lawrence Berkeley Laboratory
UNIVERSITY OF CALIFORNIA

EARTH SCIENCES DIVISION

Coupled Transport Processes in Semipermeable Media. II: Numerical Method and Results

J.S. Jacobsen and C.L. Carnahan

April 1990

Prepared for the U.S. Department of Energy under Contract Number DE-AC03-76SF00098.

DISCLAIMER

LBL–25619

Coupled Transport Processes in Semipermeable Media. Part II: Numerical Method and Results

J. S. JACOBSEN AND C. L. CARNAHAN

Earth Sciences Division, Lawrence Berkeley Laboratory
University of California, Berkeley, California

April 1990

This work was supported by the Director, Office of Energy Research, Office of Basic Energy Sciences, Engineering and Geosciences Division, of the U. S. Department of Energy under Contract No. DE–AC03–76SF00098.

TABLE OF CONTENTS

Abstract — A numerical simulator has been developed to investigate the effects of coupled processes on heat and mass transport in semipermeable media. The governing equations on which the simulator is based were derived using the thermodynamics of irreversible processes. The equations are nonlinear and have been solved numerically using the n-dimensional Newton's method. As an example of an application, the numerical simulator has been used to investigate heat and solute transport in the vicinity of a heat source buried in a saturated clay-like medium, in part to study solute transport in bentonite packing material surrounding a nuclear waste canister. The coupled processes considered were thermal filtration, thermal osmosis, chemical osmosis and ultrafiltration. In the simulations, heat transport by coupled processes was negligible compared to heat conduction, but pressure and solute migration were affected. Solute migration was retarded relative to the uncoupled case when only chemical osmosis was considered. When both chemical osmosis and thermal osmosis were included, solute migration was enhanced.

INTRODUCTION

Coupled transport processes, when they occur, cause heat and mass flows in addition to those caused by the direct processes of heat conduction, advection and diffusion. The effects of coupled processes such as osmosis and ultrafiltration have been observed in geologic settings and have been used to explain anomalous pressure and salinity data. Numerous laboratory experiments have been performed to study the effects of coupled processes on transport through clay and shale samples. CARNAHAN and JACOBSEN (1990) discuss some of the recent literature on field and experimental evidence for the occurrence of coupled processes in geologic media.

The goal of this work has been to develop a numerical simulator based on thermodynamically correct equations that describe heat and mass transport through a saturated porous medium by coupled processes. The simulator is intended to be a research tool to study *transient* heat and mass transport *within* the geologic membrane in contrast to most experimental studies that measure conditions outside the membrane after a steady state has been reached. The equations, on which the simulator is based, were derived by CARNAHAN and JACOBSEN (1990) using the thermodynamics of irreversible processes. The equations relate the rate of change of temperature, pressure and composition to heat, volume and solute fluxes. In the following section of this paper, simplified versions of the equations are presented along with the assumptions used to simplify them.

The governing equations for temperature and pressure, together with a conservation equation for solute concentration, form a system of coupled, nonlinear partial differential equations. Because of the nonlinear terms and the complexity of the system, the governing equations could not be solved analytically, but were solved numerically. The details of the numerical solution and the capabilities of the computer program that implements the numerical method are described. The program was verified by comparing the results of numerical simulations to analytical solutions of the linearized system of equations. The analytical solutions were derived by JACOBSEN and CARNAHAN (1990).

As an application of the underlying theory and the numerical simulator, the effects of the coupled processes of chemical osmosis, thermal filtration, thermal osmosis and ultrafiltration on heat and solute transport in the vicinity of a heat source buried in a saturated, clay-like material were considered. The results of simulations show the effects of the coupled processes on temperature, pressure, solute concentration and solute flux. Other potential applications include studying the transport of chemical and low-level radioactive waste contaminants in low-permeability formations and the effect of high salt concentrations on the movement of water in irrigated soils.

NOTATION

$c_{p,k}$	specific heat capacity at constant pressure of phase k, $k \equiv f, j, n$, J/(K kg).
$c_{v,k}$	specific heat capacity at constant volume of phase k, $k \equiv f, j, n$, J/(K kg).
C_0	concentration of solvent, kg/m^3.
C_s	concentration of solute s, kg/m^3.
$C_{s,m}$	average concentration of solute s, kg/m^3.
f	subscript denoting fluid phase.
J_0	solvent flux (laboratory frame of reference), kg/m^2 s.
J_q	flux of heat, W/m^2.
J_s	flux of solute s in the laboratory frame of reference, kg/m^2 s.
J_s^o	flux of solute s defined relative to motion of solvent, kg/m^2 s.
J_v	flux of volume, m^3/(m^2 s).
L_{qq}	coefficient of heat conduction (Fourier's law), W/m.
L_{qv}	coefficient of thermal filtration, m^2/s.
L_{qs}	coefficient of Dufour effect, kg/m s.
L_{sq}	coefficient of thermal diffusion, kg/m s.
L_{ss}	coefficient of mass diffusion (Fick's law), kg^2/J m s.
L_{sv}	coefficient of ultrafiltration, kg m^2/J s.
L_{vq}	coefficient of thermal osmosis, m^2/s.
L_{vs}	coefficient of chemical osmosis, kg m^2/J s.
L_{vv}	coefficient of direct advection (Darcy's law), m^4/(N s).
M_s	molecular weight of solute s, kg/mole.
n	subscript denoting nonreactive solid phase.
P	pressure, Pa.
r	radial distance, m.
R	universal gas constant, 8.314 J/K mole.
s	subscript denoting solute.
$\overline{S}_s$	partial specific entropy of solute i, J/(K kg).
t	time, s.
T	temperature, K.
T_m	average temperature, k.
$\overline{V}_s$	partial specific volume of solute, m^3/kg.
x	distance, m.
z	elevation above an arbitrary datum, m.
β_k	coefficient of thermal expansion of phase k, $k \equiv f, j, n$, K^{-1}.
Γ_1	symbol defined by (5a).
ϵ_k	volume fraction of phase k, $k \equiv f, j, n$.
κ_k	coefficient of isothermal compressibility of phase k, $k \equiv f, j, n$, m^2/N.
λ	thermal conductivity, W/(K m).
Λ_1	symbol defined by (5b).
μ_s^c	composition-dependent part of chemical potential of solute s, J/kg.
ρ_k	density of phase k, $k \equiv f, j, n$, kg/m^3.
σ_s	natural logarithm of concentration of solute s.
τ	natural logarithm of temperature.
φ_s	specific potential energy of solute s, J/m^3.

GOVERNING EQUATIONS

As an example of a physical system in which coupled transport processes arise, we consider the special case of heat and mass transport in the vicinity of a heat source buried in a semipermeable medium. For simplicity, only a single solute, denoted by a subscript s, in a one-dimensional linear or axisymmetrical (radial) coordinate system will be considered, and the following assumptions will be made:

there are no chemical reactions in the system;

gravitational and electrical forces are ignored;

the solution is ideal.

In addition, we assume that the macroscopic porosity (ϵ_f), partial specific volumes and entropies ($\overline{S}_s$ and $\overline{V}_s$, respectively), heat capacities, ($c_{p,f}$, $c_{v,f}$, $c_{v,n}$), and the coefficients of isothermal compressibility (κ_f and κ_n) and thermal expansion (β_f and β_n) are all constant. Though many of these parameters are known to vary with temperature, pressure or composition, there are not enough data available to treat them generally as continuous functions of temperature, pressure or composition.

Assuming that the macroscopic porosity, ϵ_f, is constant and that there are no chemical reactions in the system, the general equation for mass conservation, (4a) in CARNAHAN AND JACOBSEN (1990), simplifies to

$$\epsilon_f \frac{\partial C_s}{\partial t} = -\nabla J_s, \tag{1}$$

where C_s is the mass density of the solute, and J_s is the solute flux in the laboratory frame of reference.

Simplification of the governing equations for temperature and pressure, (37) and (38) in *ibid.*, (1990), requires application of all of the assumptions. By the first assumption all terms involving chemical reactions may be dropped. If gravitational and electrical forces in the system are ignored, then terms involving the gradient of the specific potential energy φ_s, defined by (39) in *ibid.*, (1990), are zero. Assuming that the solution is ideal, the gradient of the compositional part of the chemical potential, $\nabla\mu_s^c$, may be written in terms of the gradient of composition:

$$\nabla\mu_s^c = \frac{RT}{M_s}\nabla \ln C_s = \frac{RT}{C_s M_s}\nabla C_s, \tag{2}$$

where M_s is the molecular weight of solute s, R is the universal gas constant, and T is the temperature. By the fourth assumption, the gradients of $\overline{S}_s$ and $\overline{V}_s$ are zero. Employing these assumptions yields the following governing equations for temperature T and pressure P,

$$\Gamma_1 \frac{\partial T}{\partial t} = -\nabla J_q - J_v \nabla P - \frac{\beta_f T}{\kappa_f}\nabla J_v - \frac{RT}{C_s M_s} J_s^\circ \nabla C_s, \tag{3}$$

$$\Lambda_1 \frac{\partial P}{\partial t} = -\nabla J_q - J_v \nabla P - \frac{c_{p,f}\,\rho_f}{\beta_f}\nabla J_v - \frac{RT}{C_s M_s} J_s^\circ \nabla C_s. \tag{4}$$

In the equations above, J_q is the heat flux, J_v is the volume flux, and J_s° is the flux of solute s defined relative to the motion of the solvent. The symbols Γ_1 and Λ_1 are defined by

$$\Gamma_1 = \epsilon_f\,\rho_f\,c_{v,f} + \epsilon_n\,\rho_n\,c_{v,n}, \tag{5a}$$

$$\Lambda_1 = \epsilon_f \rho_f c_{v,f} \frac{\kappa_f}{\beta_f} + \epsilon_n \rho_n c_{v,n} \frac{\kappa_n}{\beta_n}. \tag{5b}$$

The mass density of the fluid phase, ρ_f, is the sum of the concentrations (mass densities) of the solvent and solute,

$$\rho_f = C_0 + C_s. \tag{6}$$

In the present work, water is the solvent, and its mass density is calculated from an equation of state involving the temperature and pressure (KELL, 1972).

The most general form of the fluxes that appear in (3) and (4) are defined by the phenomenological equations, (69), together with (70) in *ibid.*, (1990). Assuming that there are no gravitational forces in the system and that the solution is ideal, *i.e.*, that (2) is valid, leads to the following simplified forms of the phenomenological equations,

$$J_q = -L_{qq}\frac{\nabla T}{T} - L_{qv}\nabla P - L_{qs}\frac{RT}{C_s M_s}\nabla C_s, \tag{7}$$

$$J_v = -L_{vq}\frac{\nabla T}{T} - L_{vv}\nabla P - L_{vs}\frac{RT}{C_s M_s}\nabla C_s, \tag{8}$$

$$J_s^\circ = -L_{sq}\frac{\nabla T}{T} - L_{sv}\nabla P - L_{ss}\frac{RT}{C_s M_s}\nabla C_s, \tag{9}$$

where the L_{ij}, the phenomenological coefficients, are defined in the list of notation. The Onsager reciprocal relations for the phenomenological equations are

$$L_{qs} = L_{sq}, \quad L_{qv} = L_{vq}, \quad L_{vs} = L_{sv}. \tag{10}$$

The solute flux in the laboratory frame of reference, J_s, is related to J_s° by

$$J_s = C_s J_v + \left(1 - C_s \overline{V}_s\right) J_s^\circ, \tag{11}$$

and therefore,

$$\begin{aligned} J_s = &- \left[C_s L_{vq} + \left(1 - C_s \overline{V}_s\right) L_{sq}\right] \frac{\nabla T}{T} - \left[C_s L_{vv} + \left(1 - C_s \overline{V}_s\right) L_{sv}\right] \nabla P \\ &- \left[C_s L_{vs} + \left(1 - C_s \overline{V}_s\right) L_{ss}\right] \frac{RT}{C_s M_s} \nabla C_s. \end{aligned} \tag{12}$$

Both mathematical and thermodynamic coupling exist in the physical system described by equations (1), (3), (4), (7), (8) and (9). It is important to note that mathematical coupling exists in the governing equations irrespective of thermodynamic coupling. Because each governing equation involves temperature, pressure and solute concentration, even in the absence of thermodynamic coupling of transport processes, a change in temperature will affect the pressure distribution.

Thermodynamic coupling is introduced into the governing equations through the phenomenological equations (7, 8, 9), which explicitly account for the coupled processes by expressing the fluxes as sums of both direct and coupled processes. The three terms in the expression for the heat flux J_q, (7), represent the effects of

$$\text{heat conduction}, \quad -L_{qq}\frac{\nabla T}{T};$$

$$\text{thermal filtration}, \quad -L_{qv}\nabla P;$$

$$\text{diffusive-thermal effect}, \quad -L_{qs}\frac{RT}{M_s}\frac{\nabla C_s}{C_s}.$$

The expression for the volume flux J_v, (8), contains three terms representing the effects of

$$\text{thermal osmosis}, \quad -L_{vq}\frac{\nabla T}{T};$$

$$\text{advection}, \quad -L_{vv}\nabla P;$$

$$\text{chemical osmosis}, \quad -L_{vs}\frac{RT}{M_s}\frac{\nabla C_s}{C_s}.$$

The solute flux in the laboratory frame of reference J_s, (12), is comprised of six terms:

$$\text{thermal diffusion}, \quad -(1-C_s\overline{V}_s)L_{qs}\frac{\nabla T}{T};$$

$$\text{thermal osmosis}, \quad -C_sL_{vq}\frac{\nabla T}{T};$$

$$\text{ultrafiltration}, \quad -(1-C_s\overline{V}_s)L_{sv}\nabla P;$$

$$\text{advection}, \quad -C_sL_{vv}\nabla P;$$

$$\text{chemical osmosis}, \quad -L_{vs}\frac{RT}{M_s}\nabla C_s;$$

$$\text{chemical diffusion}, \quad -(1-C_s\overline{V}_s)L_{ss}\frac{RT}{M_s}\frac{\nabla C_s}{C_s}.$$

NUMERICAL METHOD OF SOLUTION

The equation set that is solved is obtained by substituting the phenomenological equations (7, 8, 9) and (12) into the governing equations (1, 3, 4). Before making the substitution, the following identities are used in the phenomenological equations:

$$\tau = \ln T, \tag{13a}$$

$$\sigma_s = \ln C_s. \tag{13b}$$

Therefore,

$$\nabla\tau = \frac{\nabla T}{T}, \tag{14a}$$

$$\nabla\sigma_s = \frac{\nabla C_s}{C_s}, \tag{14b}$$

where in the case of a one-dimensional coordinate system with space variable x,

$$\nabla^2 = \partial^2/\partial x^2, \tag{15}$$

and in the case of a radial coordinate system with space variable r,

$$\nabla^2 = \partial^2/\partial r^2 + (1/r)\partial/\partial r. \tag{16}$$

The result of substituting the phenomenological equations into the governing equations is a system of coupled, nonlinear partial differential equations in which the unknowns are the logarithm of temperature, pressure and the logarithm of solute concentration:

$$\begin{aligned}
\Gamma_1 \frac{\partial\tau}{\partial t} = {} & \left(\frac{L_{qq}}{T} + \frac{\beta_f}{\kappa_f} L_{vq}\right) \nabla^2\tau + \left(\frac{L_{qv}}{T} + \frac{\beta_f}{\kappa_f} L_{vv}\right) \nabla^2 P \\
& + \frac{R}{M_s} \left(L_{qs} + \frac{\beta_f T}{\kappa_f} L_{vs}\right) \nabla^2\sigma_s + L_{ss} T \left(\frac{R}{M_s}\right)^2 (\nabla\sigma_s)^2 \\
& + \frac{L_{vv}}{T} (\nabla P)^2 + \frac{R}{M_s} \left(L_{qs} + L_{sq} + \frac{\beta_f T}{\kappa_f} L_{vs}\right) \nabla\sigma_s \nabla\tau \\
& + \frac{R}{M_s} (L_{sv} + L_{vs}) \nabla\sigma_s \nabla P + \frac{L_{vq}}{T} \nabla P \nabla\tau,
\end{aligned} \tag{17}$$

$$\Lambda_1 \frac{\partial P}{\partial t} = \left[L_{qq} + \frac{c_{p,f}\,\rho_f}{\beta_f} L_{vq}\right] \nabla^2\tau + \left[L_{qv} + \frac{c_{p,f}\,\rho_f}{\beta_f} L_{vv}\right] \nabla^2 P$$

$$+ \frac{RT}{M_s}\left[L_{qs} + \frac{c_{p,f}\,\rho_f}{\beta_f} L_{vs}\right] \nabla^2\sigma_s + L_{ss}\left(\frac{RT}{M_s}\right)^2 (\nabla\sigma_s)^2$$

$$+ L_{vv}\,(\nabla P)^2 + \frac{RT}{M_s}\left[L_{qs} + L_{sq} + \frac{c_{p,f}\,\rho_f}{\beta_f} L_{vs}\right] \nabla\sigma_s\nabla\tau$$

$$+ \frac{RT}{M_s}\,(L_{sv} + L_{vs})\,\nabla\sigma_s\nabla P + L_{vq}\,\nabla P\nabla\tau, \tag{18}$$

$$\epsilon_f \frac{\partial\sigma_s}{\partial t} = \left[L_{vq} + \left(\frac{1}{C_s} - \overline{V}_s\right) L_{sq}\right] \nabla^2\tau + \left[L_{vv} + \left(\frac{1}{C_s} - \overline{V}_s\right) L_{sv}\right] \nabla^2 P$$

$$+ \left[L_{vs} + \left(\frac{1}{C_s} - \overline{V}_s\right) L_{ss}\right] \frac{RT}{M_s}\left[\nabla^2\sigma_s + \nabla\sigma_s\nabla\tau\right]$$

$$+ \left(L_{vq} - \overline{V}_s\, L_{sq}\right) \nabla\sigma_s\nabla\tau + \left(L_{vv} - \overline{V}_s\, L_{sv}\right) \nabla\sigma_s\nabla P$$

$$+ \left(L_{vs} - \overline{V}_s\, L_{ss}\right) \frac{RT}{M_s}\,(\nabla\sigma_s)^2\,. \tag{19}$$

The temperature and solute concentration are calculated using (13).

Each space derivative in (17), (18) and (19) is replaced by a finite-difference approximation centered in space. For example, for a finite difference grid with *variable* spacing in x, the first and second derivatives of pressure are approximated as follows:

$$\frac{\partial P_i}{\partial x} \approx \frac{1}{x_{i+1} - x_{i-1}}\left[\frac{x_i - x_{i-1}}{x_{i+1} - x_i}\,(P_{i+1} - P_i) + \frac{x_{i+1} - x_i}{x_i - x_{i-1}}\,(P_i - P_{i-1})\right], \tag{20}$$

$$\frac{\partial^2 P_i}{\partial x^2} \approx \frac{2}{x_{i+1} - x_{i-1}}\left[\frac{P_{i+1}}{x_{i+1} - x_i} - \frac{(x_{i+1} - x_{i-1})\,P_i}{(x_{i+1} - x_i)\,(x_i - x_{i-1})} + \frac{P_{i-1}}{x_i - x_{i-1}}\right]. \tag{21}$$

In the equations above, the subscripts refer to nodes of the finite-difference grid: x_i is the value of x at the i^{th} node, and P_i is the pressure at x_i. Note that in the case of uniform grid spacing, $x_{i+1} - x_i = x_i - x_{i-1} = \Delta x$, and the finite-difference expressions in (20) and (21) reduce to the familar centered difference forms.

The time derivatives in (17) through (19) are replaced by finite-difference approximations that are projected forward in time:

$$\frac{\partial P}{\partial t} \approx \frac{P^{j+1} - P^j}{\Delta t}, \tag{22}$$

where the time step size Δt is given by

$$\Delta t = t^{j+1} - t^j, \tag{23}$$

and the superscripts are the indices of the time steps.

After the partial derivatives are replaced by finite-difference approximations, the system of governing equations becomes a set of nonlinear algebraic equations. The nonlinearities in the governing equations are of two types: products of first derivatives and factors of temperature or solute concentration or both multiplying derivative terms. Because of the nonlinearity of the governing equations, an iterative method, the n-dimensional Newton's method (NDNM) (ORTEGA and RHEINBOLDT, 1970) was chosen to solve the system of equations. The NDNM, also known as the Newton-Raphson method, is a generalization of Newton's method, which is used to find the root (or roots) of a one-dimensional nonlinear equation. The NDNM iteratively determines a vector of values that satisfy a system of homogeneous equations known as the residue equations. In this work, the elements of the vector of unknowns are the values of τ, P and σ_s at different locations in space, and the residue equations are the finite-difference approximations of the governing equations rewritten as homogeneous equations.

The NDNM can be written as

$$\mathbf{u}^{k+1} = \mathbf{u}^k - [F'(\mathbf{u}^k)]^{-1} F(\mathbf{u}^k), \tag{24}$$

where $\mathbf{u}$ is the vector of unknowns, $F(\mathbf{u}^k)$ is the vector of residue equations and $F'(\mathbf{u}^k)$ is the Jacobian matrix. The elements of the Jacobian matrix are determined by differentiating each residue equation with respect to all of the unknowns. In practice the inverse of the Jacobian matrix in (24) is not computed, but rather the linear system,

$$F'(\mathbf{u}^k)\mathbf{w} = -F(\mathbf{u}^k), \tag{25}$$

is solved for $\mathbf{w}$, and then the $(k+1)$–th iterate is calculated from

$$\mathbf{u}^{k+1} = \mathbf{u}^k + \mathbf{w}. \tag{26}$$

For one-dimensional flow, the Jacobian matrix in (25) is block tridiagonal in structure. Therefore, the linear system in (25) can be solved easily and accurately using the method of L–U factorization, which has been specialized by HINDMARSH (1977) to factor a block tridiagonal matrix.

The NDNM was chosen because it is widely used to solve nonlinear systems of equations (MILLER and BENSON, 1983; ABRIOLA and PINDER, 1985; CARNAHAN, 1987), conceptually easy to implement and second-order convergent (DAHLQUIST and BJÖRCK, 1974, p. 224). Other numerical methods were considered. For example, the NDNM was chosen over Steffensen's method (ISAACSON and KELLER, 1966), which is also second-order convergent, because the NDNM takes fewer operations. Steffensen's method is a derivative-free method, that is, it does not involve the Jacobian matrix, but instead requires two evaluations of the set of residue equations at each iteration. The NDNM requires one evaluation of the set of residue equations and one evaluation of the Jacobian matrix. There are, however, fewer operations involved in evaluating the Jacobian matrix than in evaluating the set of residue equations. Ideally, one would like to be able to apply more than one method to a problem in order to see which method performs better, since the performance of an algorithm is problem-dependent. CUYT and RALL (1985) used Newton's method and another iterative method named Halley's method to solve two systems of nonlinear equations and found that Newton's method performed better for one of the systems and Halley's method (CUYT and RALL, 1985) performed better for the other. Unfortunately, time and budget constraints rarely allow the researcher the luxury of comparing different numerical methods of solution.

For the NDNM to be second-order convergent, the elements of the Jacobian matrix must be determined analytically by differentiating the residue equations. If the elements of the Jacobian matrix are calculated numerically, using divided differences for example, then the order of convergence is less than second-order (ISAACSON and KELLER, 1966, pp. 98, 101). A great deal of effort was involved in determining the Jacobian elements analytically and coding the expressions for them, but the effort was made in order to decrease computation time and achieve second-order convergence.

Computation time could also be decreased by implementing acceleration methods such as an n-dimensional version of Aitken's δ^2 method (ISAACSON and KELLER, 1966) or by constructing hybrid methods, which combine computationally inexpensive methods such as the secant method with more powerful methods like Newton's method. A simpler way to decrease the computation time of the NDNM is to not evaluate the Jacobian matrix at every iteration. Because such a change would decrease the order of convergence as well, it could conceivably increase the total computation time. In the present application of the NDNM, the method converges within a few iterations at each time step, so the possible trade-off between decreased computation time and a slower rate of convergence does not seem worth pursuing.

DESCRIPTION OF THE NUMERICAL SIMULATOR

The numerical method of solution described above has been incorporated into a computer program named TIP, which is an acronym for the thermodynamics of irreversible processes. TIP was developed at Lawrence Berkeley Laboratory except for a set of subroutines, written by A. HINDMARSH (1977), used to perform the L–U factorization and solve the linear system in (25). The TIP program is written in FORTRAN and was developed to run on the Cray X-MP computer at the National Magnetic Fusion Energy Computer Center at Lawrence Livermore National Laboratory. The program was carefully coded in order to utilize the high-speed vector and floating-point functional units of the Cray X-MP.

Capabilities of TIP

At this time the TIP program can handle transport in only one dimension, though the geometry of the system may be either linear or radial. The spacing of the finite difference grid may be either constant or may increase with distance. The latter choice allows for a very fine grid spacing near the inner boundary where the gradients of temperature, pressure and solute concentration are the largest and a coarse grid spacing at the outer boundary where the gradients are much smaller. The variable grid spacing makes simulation of a semi-infinite medium possible: the outer boundary can be placed far enough from the inner boundary to minimize the effects of the outer boundary conditions on the solutions without greatly increasing the number of nodes in the finite difference grid.

The TIP program can handle a variety of initial and boundary conditions. The initial condition for a variable can be constant value, constant gradient or the values at the inner and outer boundary can be specified and the program will determine the gradient. Only constant-flux (Neumann) boundary conditions are allowed at the inner boundary. At the outer boundary, either a constant-value (Dirichlet) or zero-gradient (Neumann) condition may be imposed. Implementation of the constant-flux boundary condition is described in Appendix A.

Limitations of TIP

Some of the limitations of the TIP program result from assumptions made when deriving the governing equations. Limitations that could be overcome by modifying the computer program are that the medium is assumed to be homogeneous, the boundary conditions are constant in time and only one solute is allowed. Though there is a scarcity of data on how the material properties of a medium vary with temperature and composition, constant material properties for more than one medium could be used to simulate layered media. The addition of time-dependent boundary conditions is important in order to be able to simulate mass transport away from a heat source in the presence of an already established temperature field. Allowance for more than one solute is needed in order to eventually incorporate chemical reactions.

There are several problems involved in using an equation of state to calculate the solvent concentration. First, the equation of state in use (KELL, 1972) is for pure water, and therefore, is a good approximation only for low solute concentrations*. In addition there are temperature and pressure limits on the present equation of state. It is valid only for temperatures in the range of 0 to 150°C and for

* An equation of state for aqueous sodium chloride has been developed by ROGERS and PITZER (1982) (see also PITZER, PEIPER and BUSEY, 1984) and may be implemented in the TIP program in the future.

pressures less than 1 kbar (10^8 Pa). Finally, the amount of solvent in the system is not conserved, that is, there is no direct link between the amount of solvent calculated by the equation of state and an increase in the solvent concentration that would result from a release of solvent at the boundary. This is not a serious shortcoming, however, because the solvent concentration enters into the governing equations (4, 5) only through ρ_f, the fluid density, defined by (6). For the values of the input parameters used (see Table 3 in the following section), variations in ρ_f have a small effect on the magnitude of the factors Γ_1 in (4) and Λ_1 in (5). The effect of variations in Γ_1 and Λ_1 on the results of the numerical simulations is even smaller.

Verification of TIP

The TIP program has been verified by comparing the results of numerical simulations in which the nonlinear governing equations, (17), (18) and (19), are solved to analytical solutions derived for the system of linear governing equations. To make the equations linear, all products of derivatives were omitted, and factors of temperature and solute concentration were replaced by average values, $C_{s,m}$ and T_m:

$$\Gamma_1 \frac{\partial T}{\partial t} = \left(\frac{L_{qq}}{T_m} + \frac{\beta_f}{\kappa_f} L_{vq}\right) \nabla^2 T + \left(L_{qv} + \frac{\beta_f T_m}{\kappa_f} L_{vv}\right) \nabla^2 P + \frac{R T_m}{C_{s,m} M_s} \left(L_{qs} + \frac{\beta_f T_m}{\kappa_f} L_{vs}\right) \nabla^2 C_s, \tag{27}$$

$$\Lambda_1 \frac{\partial P}{\partial t} = \frac{1}{T_m} \left(L_{qq} + \frac{c_{p,f}\, \rho_f}{\beta_f} L_{vq}\right) \nabla^2 T + \left(L_{qv} + \frac{c_{p,f}\, \rho_f}{\beta_f} L_{vv}\right) \nabla^2 P + \frac{R T_m}{C_{s,m} M_s} \left(L_{qs} + \frac{c_{p,f}\, \rho_f}{\beta_f} L_{vs}\right) \nabla^2 C_s, \tag{28}$$

$$\epsilon_f \frac{\partial C_s}{\partial t} = \frac{1}{T_m} \left[C_{s,m} L_{vq} + (1 - C_{s,m} \overline{V}_s) L_{sq}\right] \nabla^2 T + \left[C_{s,m} L_{vv} + (1 - C_{s,m} \overline{V}_s) L_{sv}\right] \nabla^2 P + \left[C_{s,m} L_{vs} + (1 - C_{s,m} \overline{V}_s) L_{ss}\right] \frac{R T_m}{C_{s,m} M_s} \nabla^2 C_s. \tag{29}$$

Solutions to these equations were derived for a one-dimensional geometry in a semi-infinite domain for the uncoupled and all of the coupled cases. At the inner boundary, nonzero heat, solute and solvent fluxes were imposed. At the outer boundary, *i.e.*, at infinity, all of the variables were set equal to their initial values. For a radial geometry, solutions in the Laplace transform space were derived for the uncoupled and all coupled cases for the same boundary conditions as those of the one-dimensional geometry. It is possible to analytically invert the solutions in the Laplace transform space, but because the inverted solutions involve infinite integrals of Bessel function cross products, it is computationally more efficient to invert them numerically. An algorithm given by H. STEHFEST (1970) can be used to numerically invert them. The solutions for the one-dimensional geometry and the solutions in the Laplace transform space for the radial geometry are available in a separate report (JACOBSEN and CARNAHAN, 1990).

Agreement between the analytical solutions and the numerical solutions to the governing equations (17), (18) and (19) is excellent at early simulated times for both linear and radial geometries. As examples

of this, Figs. 1 and 2 compare temperature, pressure and solute profiles, calculated using the analytical and numerical solutions, at simulated times of one and ten years in an annulus of semipermeable material surrounding a source of heat and solute. (The system being simulated and the parameters used in the simulations are the same as those described in more detail in the following section.) Figures 1a, 1b and 1c compare the analytical and numerical simulations for the case in which coupling has been neglected. Figures 2a, 2b and 2c show results for the case when chemical osmosis, ultrafiltration, thermal osmosis and thermal filtration have been included. For the system simulated in Figs. 1 and 2, at times later than ten years there are discrepancies between the analytical and numerical solutions because the magnitudes of the nonlinear terms in the governing equations that are solved numerically increase with time in comparison to the linear terms.

The analytical solutions also have been useful in predicting the maximum temperature rise for a given incoming heat flux and in determining how large to make the finite difference grid. A large heat flux could cause the temperature to increase above the upper limit for the equation of state thereby invalidating the simulation results. Changes in pressure propagate very quickly through the system; the pressure front is always far ahead of both the temperature and solute fronts. It is important, therefore, to be able to estimate for the maximum simulation time the smallest distance at which the pressure remains undisturbed.

The performance of the TIP code is checked also during each simulation by examining the solute mass balance at every time step for which results are printed. The amount of solute in the system is calculated using the trapezoidal rule (DAHLQUIST and BJÖRCK, 1974) and compared to the sum of the amount of solute initially in the system and that introduced by the flux boundary condition. For most simulations, the discrepancy between the calculated and predicted amounts of solute is less than three percent, even at simulated times of 1000 years representing several thousand iterations. Larger discrepancies have been observed in simulations where boundary effects were caused by finite difference grids too small in extent or where large heat fluxes caused the temperature to increase outside of the range of validity of the equation of state.

RESULTS FROM NUMERICAL SIMULATIONS

Table 1 lists the driving forces and the fluxes that may be significantly affected by the coupled processes when the coefficients of chemical osmosis and ultrafiltration are nonzero, which hereafter will be referred to as the *chemical osmosis case.* Note that the reciprocal relations (10) require the coupled processes to occur in *pairs.*

Table 1. Effects of Chemical Osmosis and Ultrafiltration (Chemical Osmosis Case)

coupled effect	force	flux(es) affected
chemical osmosis	solute gradient	volume and solute fluxes
ultrafiltration	pressure gradient	solute flux

The forces and fluxes corresponding to the coupled effects arising from nonzero values of the coefficients of thermal osmosis and thermal filtration, the *thermal osmosis case*, are listed in Table 2.

Table 2. Effects of Thermal Osmosis and Thermal Filtration (Thermal Osmosis Case)

coupled effect	force	flux(es) affected
thermal filtration	pressure gradient	heat flux
thermal osmosis	temperature gradient	volume and solute fluxes

In the thermal osmosis case, the temperature, pressure and solute distributions may differ from those of the case without coupling. In the chemical osmosis case, the pressure distribution and solute concentration may differ from those of the uncoupled case.

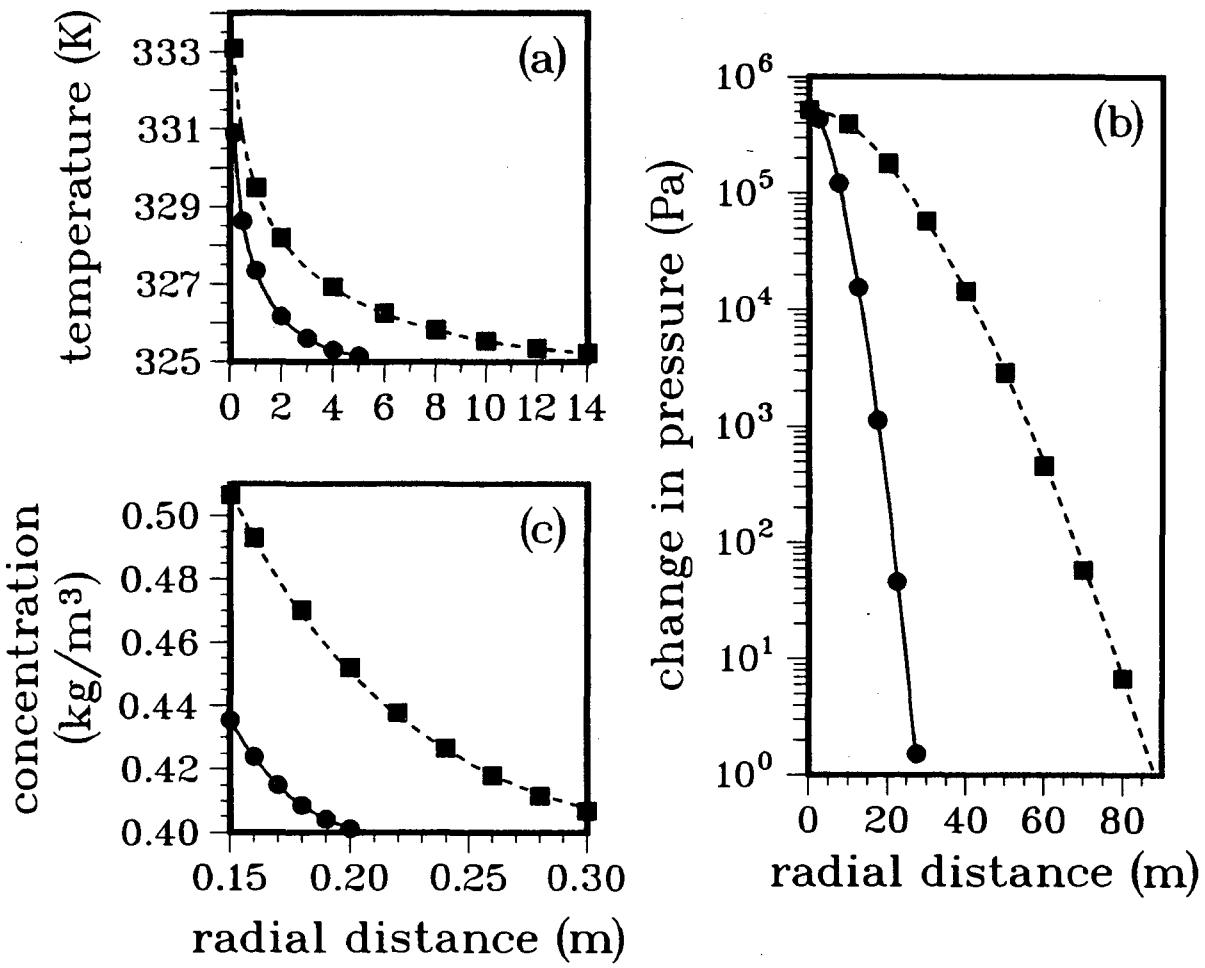

Figure 1. Comparison of analytical and numerical solutions at simulation times of 1 and 10 years. Coupled processes not included. Solid line – numerical solution, one year; dashed line – numerical solution, ten years; • – analytical solution, one year; ■ – analytical solution, ten years. (a) temperature, (b) change in pressure, (c) solute concentration.

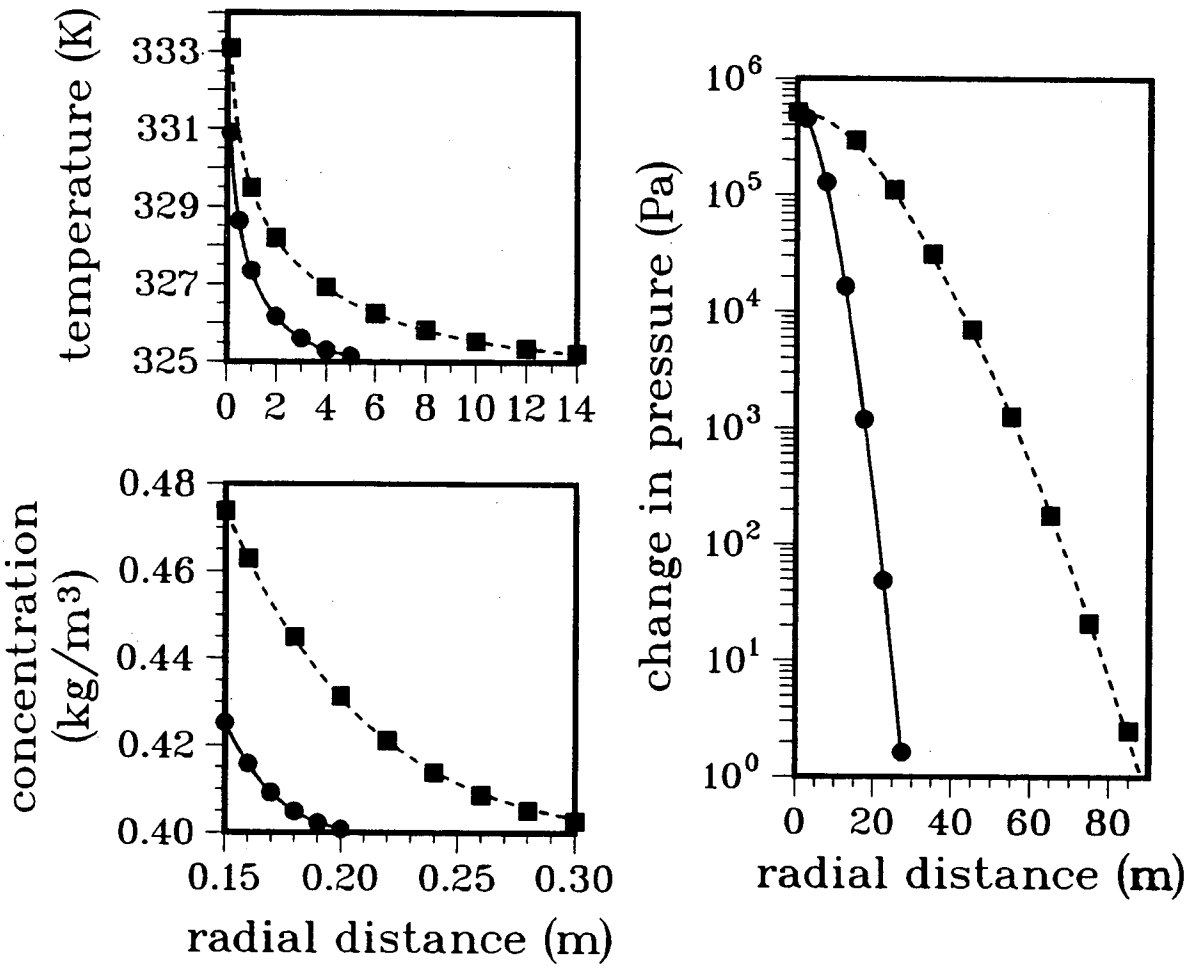

Figure 2. Comparison of analytical and numerical solutions at simulation times of 1 and 10 years. Chemical osmosis, ultrafiltration, thermal osmosis and thermal filtration included. Solid line – numerical solution, one year; dashed line – numerical solution, ten years; • – analytical solution, one year; ■ – analytical solution, ten years. (a) temperature, (b) change in pressure, (c) solute concentration.

The heat flux is not listed as one of the fluxes affected by chemical osmosis. The temperature distribution for the chemical osmosis case could, nevertheless, differ from that of the uncoupled case not as a result of thermodynamic coupling, but of the mathematical coupling that exists in the governing equations. This distinction points out the difficulty in trying to determine the effect of a thermodynamically coupled process on one of the quantities of interest. The heat, solute and volume fluxes are the most direct measures of the effects of coupled processes on the system and should be examined when trying to understand the effects of coupled processes on heat and solute transport.

The magnitudes of the effects of coupling depend on the phenomenological coefficients and on the gradients of temperature, pressure and solute concentration. The gradients partly depend on the incoming heat, solute and solvent fluxes. Large values of the incoming fluxes may, depending on the properties of the medium, produce large gradients of temperature, solute concentration and pressure. Because of the flux boundary conditions imposed on the simulations discussed here, the heat, solute and solvent fluxes for all of the uncoupled and coupled cases are the same at the inner boundary regardless of the magnitudes of the individual driving forces (gradients). Differences in the fluxes due to coupled processes are apparent at short distances from the boundary.

The objectives of the numerical simulations are to assess the effects of coupling on distributions of temperature, pressure and solute concentration and on solute fluxes. The effects are assessed by comparison with results of simulations without coupling. Effects of varying the magnitudes of the coupling coefficients are examined also. In this work only chemical osmosis and thermal osmosis were considered because these are likely to be the two most important coupled processes in the vicinity of a heat source buried in a saturated, semipermeable medium.

Phenomenological Coefficients

The parameters used in the simulations are given in Table 3, except where noted in the text. The values of the phenomenological coefficients were taken from published data on bentonite (LETEY and KEMPER, 1969; MOSS and MOLECKE, 1983) and on kaolinite (SRIVASTAVA and AVASTHI, 1975). Values of L_{vv} and L_{vs} $(= L_{sv})$ were calculated from the values of similar coefficients measured by LETEY and KEMPER (1969). Values of L_{vv} and L_{vq} $(= L_{qv})$ were calculated from the data of SRIVASTAVA and AVASTHI (1975) on kaolinite. The correspondence between the phenomenological coefficients used in this work and those of the authors mentioned above may be determined by comparing LETEY and KEMPER'S equations (6) and (7) to equations (8) and (9) in this paper and SRIVASTAVA and AVASTHI'S equations (2) and (3) to (8) and (7), respectively. A value of L_{vq} for bentonite was estimated using the value of L_{vv} for bentonite from LETEY and KEMPER'S data and assuming that the ratio of L_{vq} to L_{vv} is approximately the same for bentonite as for kaolinite. The value of L_{qq} used in the simulations was estimated from $L_{qq} \approx \lambda T$ using measurements of thermal conductivity (λ) of bentonite made by MOSS and MOLECKE (1983).

Initial and Boundary Conditions

Constant value initial conditions were used for all of the variables. The initial temperature was 325 K, the initial pressure was 10^7 Pa, and the initial solute concentration was 0.4 kg/m^3. At the outer boundary, all variables were fixed at their initial values during the simulations. The finite difference grid was designed to be large enough to simulate transport in an axisymmetrical, semi-infinite medium: a grid radius of 1500 m was used. The size of the grid was estimated using the analytical solution for the pressure distribution, since changes in pressure propagate far more rapidly than changes in either temperature or solute concentration. A variable grid spacing, with finer spacing near the flux boundary located at $r = 0.15$ m, was used in order to preserve solution accuracy near the inner boundary and to limit the number of grid points. Constant flux boundary conditions were imposed at the inner boundary: a value of 10 W/m^2 was used for the heat flux, 10^{-11} kg/m^2·s for the solute flux, and the solvent flux was zero. While flux boundary conditions are more realistic in this case than constant temperature and constant concentration boundary conditions, they are simplistic because the heat output of a nuclear waster canister would decrease in time due to radioactive decay, and chemical reactions taking place in the waste form would control the rate of solute release.

Table 3. Parameter Values Used in Numerical Simulations

initial conditions:

$C_0 = 10^3$ kg/m^3
$C_s = 0.4$ kg/m^3
$P = 10^7$ N/m^2
$T = 325$ K

flux conditions at inner boundary:

$J_0 = 0$ kg/m^2 s
$J_q = 10$ W/m^2, radial geometry
$J_s = 10^{-11}$ kg/m^2 s

phenomenological coefficients:

$L_{qq} = 2.6 \times 10^2$ W/m
L_{qv} – varied (see text and figures), m^2/s
L_{qs} – varied (see text and figures), kg/m s
L_{sq} – varied (see text and figures), kg/m s
$L_{ss} = 6.8 \times 10^{-17}$ kg^2/J m s
L_{sv} – varied (see text and figures), kg m^2/J s
L_{vq} – varied (see text and figures), m^2/s
L_{vs} – varied (see text and figures), kg m^2/J s
$L_{vv} = 2.4 \times 10^{-16}$ m^5/J s

other parameters:

$c_{p,f} = 5.0 \times 10^3$ J/kg K
$c_{v,f} = 4.2 \times 10^3$ J/kg K
$c_{v,n} = 1.3 \times 10^3$ J/kg K
$M_s = 5.844 \times 10^{-2}$ kg/mole
$R = 8.314$ J/K mole
$\overline{V}_s = 2.9 \times 10^{-4}$ m^3/kg
$\beta_f = 4.7 \times 10^{-4}$ K^{-1}
$\beta_n = 3.0 \times 10^{-5}$ K^{-1}
$\epsilon_f = 0.3$
$\epsilon_n = 0.7$
$\kappa_f = 4.4 \times 10^{-10}$ m^2/N
$\kappa_n = 2.8 \times 10^{-11}$ m^2/N
ρ_f – calculated, kg/m^3
$\rho_n = 2.5 \times 10^3$ kg/m^3

Comparison of Uncoupled and Coupled Cases

This section compares the temperature, pressure and solute concentrations calculated for the uncoupled case and three cases of coupling: chemical osmosis, thermal osmosis and combined chemical osmosis and thermal osmosis. All results are shown at a simulated time of 1000 years.

Temperature and Gradient of Temperature. Thermal filtration is the only coupled process considered that directly affects the transport of heat. For the times simulated, 1000 years or less, the temperature profiles for the uncoupled and all of the coupled cases coincide (Fig. 3). *For the choice of parameters and incoming heat flux used,* this result shows that in the coupled cases considered, the transport of heat is unaffected by coupling, and in particular, that thermal filtration is negligible relative to the direct process of heat conduction.

That the transport of heat is unaffected by coupling for the set of parameters in Table 3 can be understood in part by looking at the expression for the heat flux. Ignoring thermal diffusion ($L_{qs} = 0$), (7) becomes

$$J_q = -L_{qq}\frac{\nabla T}{T} - L_{qv}\nabla P. \tag{30}$$

The second term contributes to J_q only when thermal osmosis is included. Comparing the magnitudes of L_{qq} and L_{qv}, $L_{qq} = 2.6 \times 10^2$ W/m and $L_{qv} = 3.8 \times 10^{-10}$ m^2/s, it can be seen that the pressure gradient must be extremely large for the second term to contribute to J_q. Based on simulation results, it appears that for all cases the dominant term in (4) is the second derivative of temperature. Though the temperature is unaffected by coupling in the present cases, it is possible that a change in material properties, phenomenological coefficients or incoming heat flux could result in temperature differences between the uncoupled and coupled cases.

Pressure and Gradient of Pressure. Unlike the temperature, the pressure distribution is sensitive to the effects of coupling. Figure 4 shows the change in pressure from an initial pressure of 10^7 Pa. The pressure profiles show obvious, but small, differences. The differences are largest near the inner boundary where the pressure profiles for each case are distinct. After a distance of about 2 m, the pressure profiles for the uncoupled and chemical osmosis cases coincide and those for the thermal osmosis and combined chemical osmosis and thermal osmosis cases coincide. The difference between the two pairs of profiles continues for a distance of nearly 100 m.

Though the differences in the pressure distributions for the uncoupled and coupled cases are quite small, the resulting differences in the pressure gradients vary in sign and by several orders of magnitude (Fig. 5). The pressure gradients for the thermal osmosis and combined chemical osmosis and thermal osmosis cases are positive and similar in magnitude near the inner boundary. The pressure gradients for the uncoupled and chemical osmosis cases are negative, but nearly four orders of magnitude apart. Differences in the pressure gradients are important because the pressure gradient is the driving force for the advective solute flux in *all* uncoupled and coupled cases and for additional heat and solute fluxes in the coupled cases. Thermal filtration causes an additional heat flux when L_{qv} is nonzero, and ultrafiltration causes an additional solute flux when L_{sv} is nonzero. In the cases presently being considered, the differences in the pressure gradients are large enough to be significant in some coupled cases, but not others.

Solute Concentration. The coupled processes affect the movement of solute and cause differences among the solute concentrations for the uncoupled and coupled cases. The solute profiles for the uncoupled, chemical osmosis and combined chemical osmosis and thermal osmosis cases are distinct near the inner boundary (Fig. 6). The profile for the thermal osmosis case coincides with the uncoupled case in

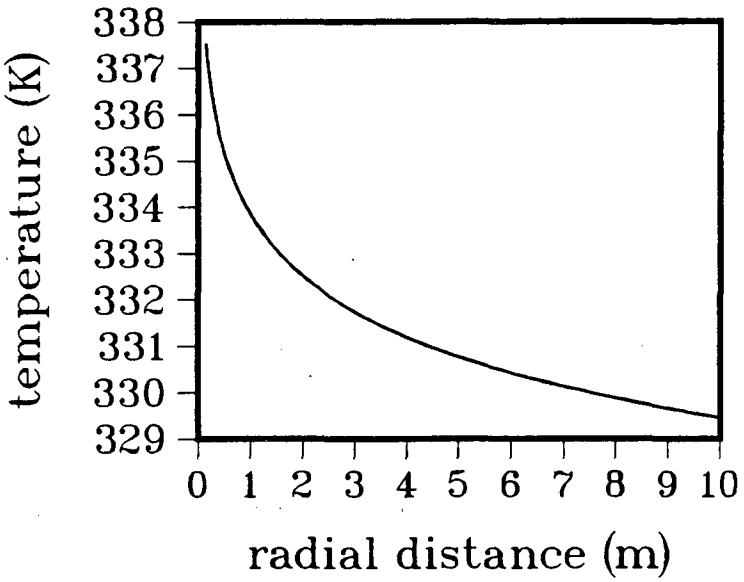

Figure 3. Temperature distribution at a simulation time of 1000 years with and without coupling. Initial temperature of 325 K, incoming heat flux of 10 W/m^2, $L_{qv} = L_{vq} = 3.8 \times 10^{-10}$ m^2/s, $L_{vs} = L_{vs} = -8 \times 10^{-17}$ kg m^2/J s. *All curves coincide.*

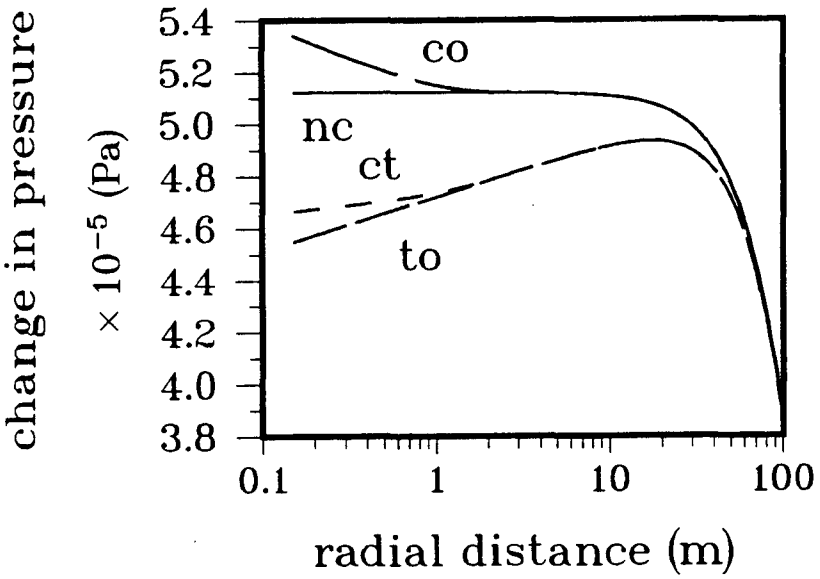

Figure 4. Change in pressure at a simulation time of 1000 years with and without coupling. Initial pressure of 10^7 Pa, $L_{qv} = L_{vq} = 3.8 \times 10^{-10}$ m^2/s, $L_{vs} = L_{vs} = -8 \times 10^{-17}$ kg m^2/J s. **nc** – no coupling, **co** – chemical osmosis and ultrafiltration included, **to** – thermal osmosis and thermal filtration included, **ct** – all coupled processes included in **co** and **to** cases.

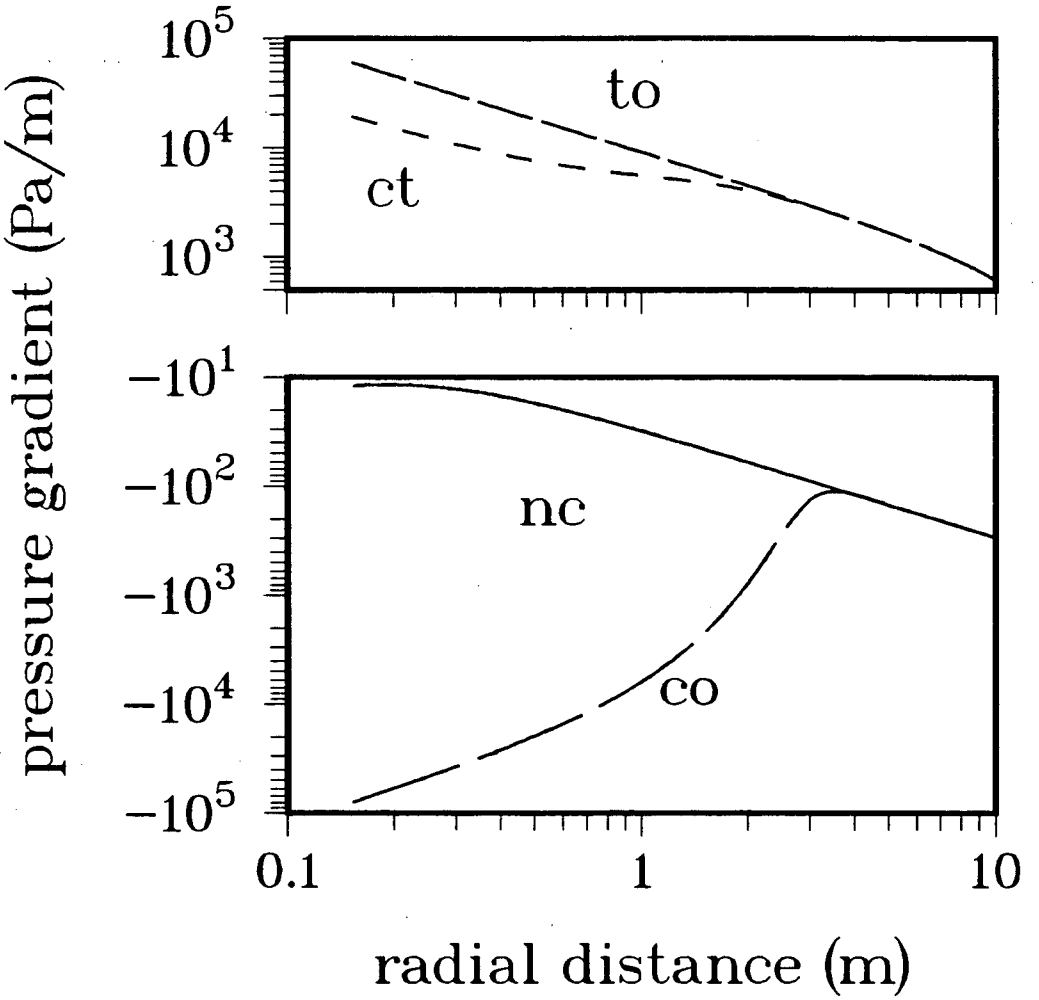

Figure 5. Pressure gradient at a simulation time of 1000 years with and without coupling. Initial pressure of 10^7 Pa, $L_{qv} = L_{vq} = 3.8 \times 10^{-10}$ m^2/s, $L_{vs} = L_{vs} = -8 \times 10^{-17}$ kg m^2/J s. **nc** – no coupling, **co** – chemical osmosis and ultrafiltration included, **to** – thermal osmosis and thermal filtration included, **ct** – all coupled processes included in **co** and **to** cases.

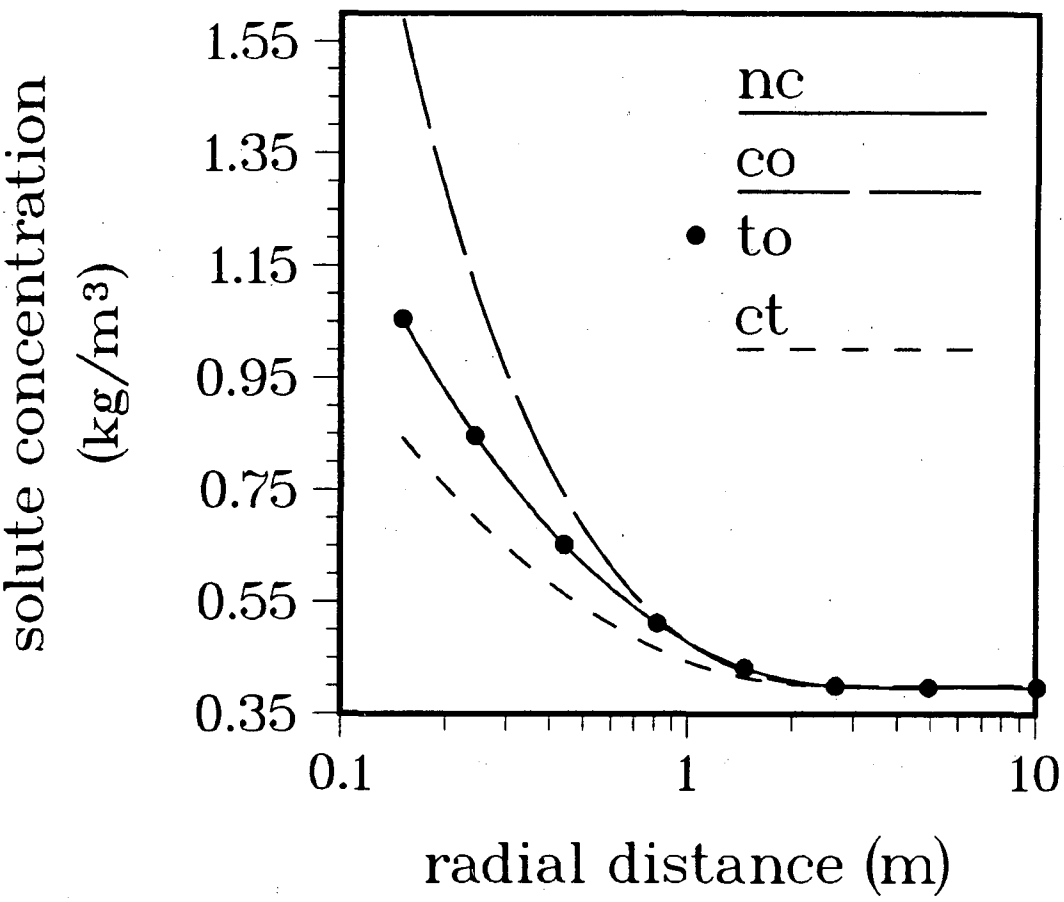

Figure 6. Solute concentration at a simulation time of 1000 years with and without coupling. Initial solute concentration of 0.4 kg/m^3, incoming solute flux of 10^{-11} kg/m^{2}s, $L_{qv} = L_{vq} = 3.8 \times 10^{-10}$ m^2/s, $L_{vs} = L_{vs} = -8 \times 10^{-17}$ kg m^2/J s. **nc** – no coupling, **co** – chemical osmosis and ultrafiltration included, **to** – thermal osmosis and thermal filtration included, **ct** – all coupled processes included in **co** and **to** cases.

this region, and thereafter all of the profiles converge. Near the flux boundary, the concentration for the chemical osmosis case is about 50% larger than that for the uncoupled case. The concentration for the combined chemical osmosis and thermal osmosis case is about 20% less than that of the uncoupled case or about 50% of the chemical osmosis case.

Given that the pressure gradients, and hence the advective fluxes, for the uncoupled and thermal osmosis cases differ in sign (Fig. 5), it is surprising that the concentration profiles for those cases are the same. In the governing equation for solute for the thermal osmosis case, the larger terms involving the pressure gradient are offset by thermal osmosis terms resulting in identical concentration profiles for the uncoupled and thermal osmosis cases.

A second unexpected but important feature of the concentration profiles is the magnitude of the concentration in the combined chemical osmosis and thermal osmosis case relative to those for the other coupled cases. As noted above the profiles for the uncoupled and thermal osmosis cases coincide implying that thermal osmosis (for the set of parameters used) does not affect solute tranport. This is clearly not the case when chemical osmosis has been included also. Near the flux boundary, the concentration for the combined chemical osmosis and thermal osmosis case is only 50% of the concentration for the chemical osmosis case. Whereas chemical osmosis results in a larger solute concentration than that predicted by the uncoupled case, when chemical osmosis and thermal osmosis are both included, the combined coupled processes result in a smaller solute concentration implying faster solute migration away from the boundary than predicted by the direct processes of advection and diffusion.

Solute Fluxes. The solute flux is the most direct measure of solute migration. The concentration profile shows how much solute is in the system, but the solute flux shows the rate of movement of the solute. Furthermore, looking at the individual solute fluxes that contribute to the total solute flux shows the forces that cause the solute to migrate. When chemical osmosis and thermal osmosis are included, the total solute flux in the laboratory frame of reference is given by

$$J_s = - C_s L_{vq} \frac{\nabla T}{T} - [C_s L_{vv} + (1 - C_s \overline{V}_s) L_{sv}] \nabla P - [C_s L_{vs} + (1 - C_s \overline{V}_s) L_{ss}] \frac{RT}{M_s C_s} \nabla C. \qquad (31)$$

thermal osmosis — advection — ultrafiltration — chemical osmosis — chemical diffusion

The advective flux and diffusive flux contribute to the total solute flux in all of the coupled cases. In the uncoupled case, the total flux is comprised of only those two fluxes. When chemical osmosis is included, there are additional contributions to the total flux by the chemical osmotic flux and the ultrafiltrative flux. When thermal osmosis is included, the thermal osmotic flux also adds to the total flux.

Looking at the solute fluxes for the uncoupled and thermal osmosis cases, Figs. 7 and 8, the diffusive fluxes, which are proportional to the solute gradients, are identical because the concentration profiles for the two cases are the same. The advective fluxes are dissimilar because the pressure gradients differ as described earlier. Within a radius of two meters of the flux boundary, the total flux in the uncoupled case is approximately equal to the diffusive flux (Fig. 7). In the thermal osmosis case (Fig. 8), three fluxes contribute to the total flux: the thermal osmotic flux, the advective flux and the diffusive flux. The thermal osmotic flux is of the same order of magnitude and sign as the diffusive flux, but the advective flux, which is negative, opposes the thermal osmotic flux and cancels its contribution to the total flux. In the chemical osmosis case, Fig. 9, the advective and chemical osmotic fluxes cancel, and within a two-meter radius, the total flux is equal to the sum of the (positive) diffusive and (negative) ultrafiltrative fluxes.

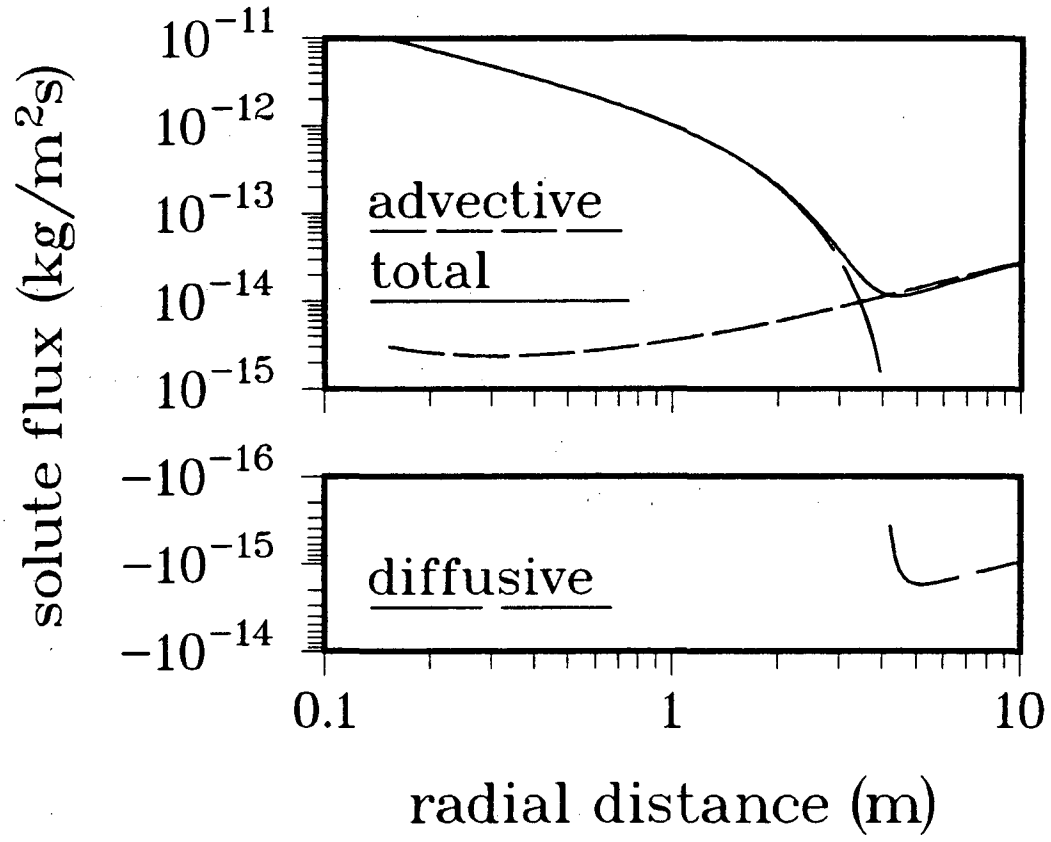

Figure 7. Individual and total solute fluxes at a simulation time of 1000 years. Coupled processes not included. Incoming solute flux of 10^{-11} kg/m^2 s.

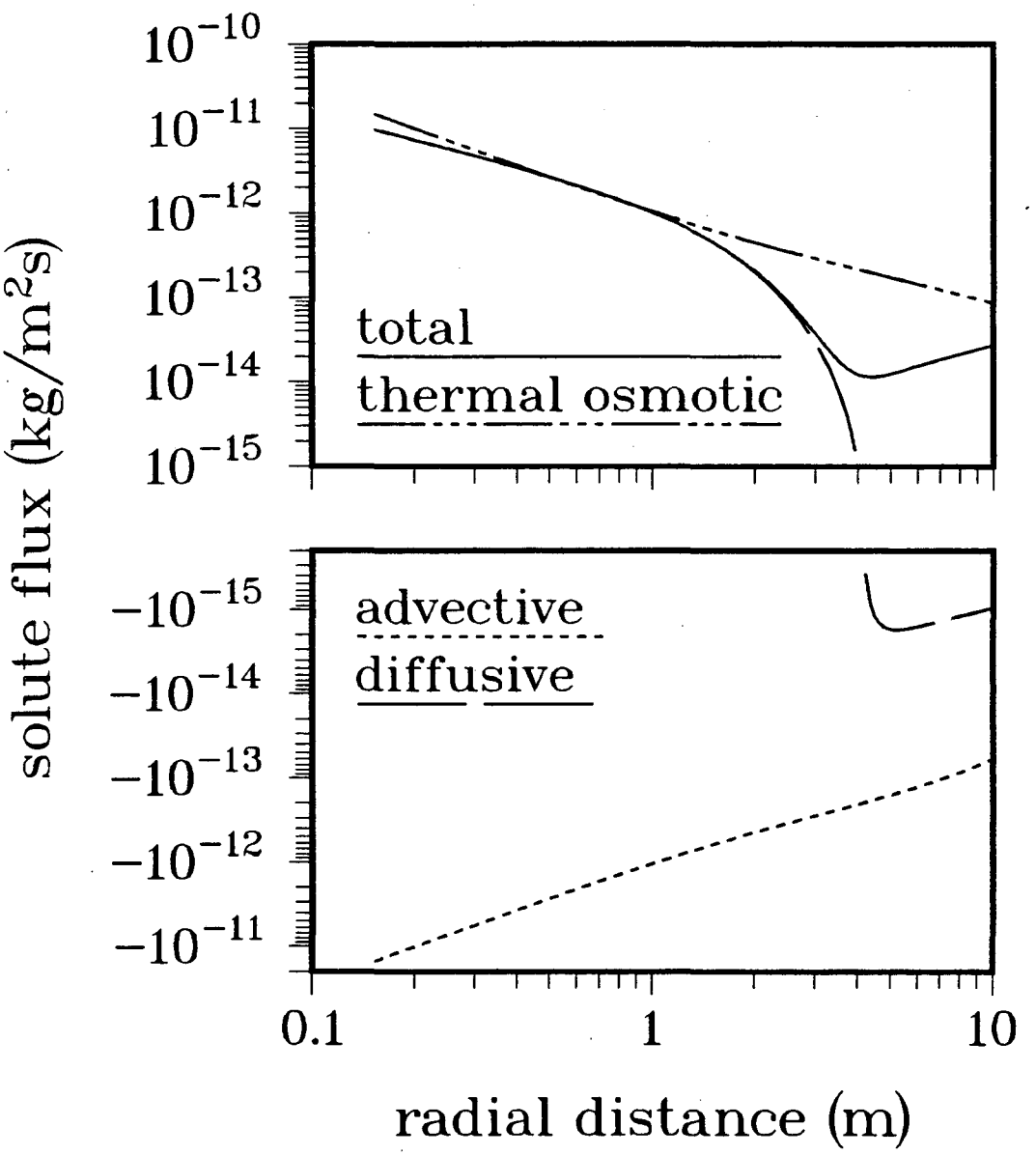

Figure 8. Individual and total solute fluxes at a simulation time of 1000 years. Thermal osmosis and thermal filtration included. Incoming solute flux of 10^{-11} kg/m^2 s, $L_{qv} = L_{vq} = 3.8 \times 10^{-10}$ m^2/s.

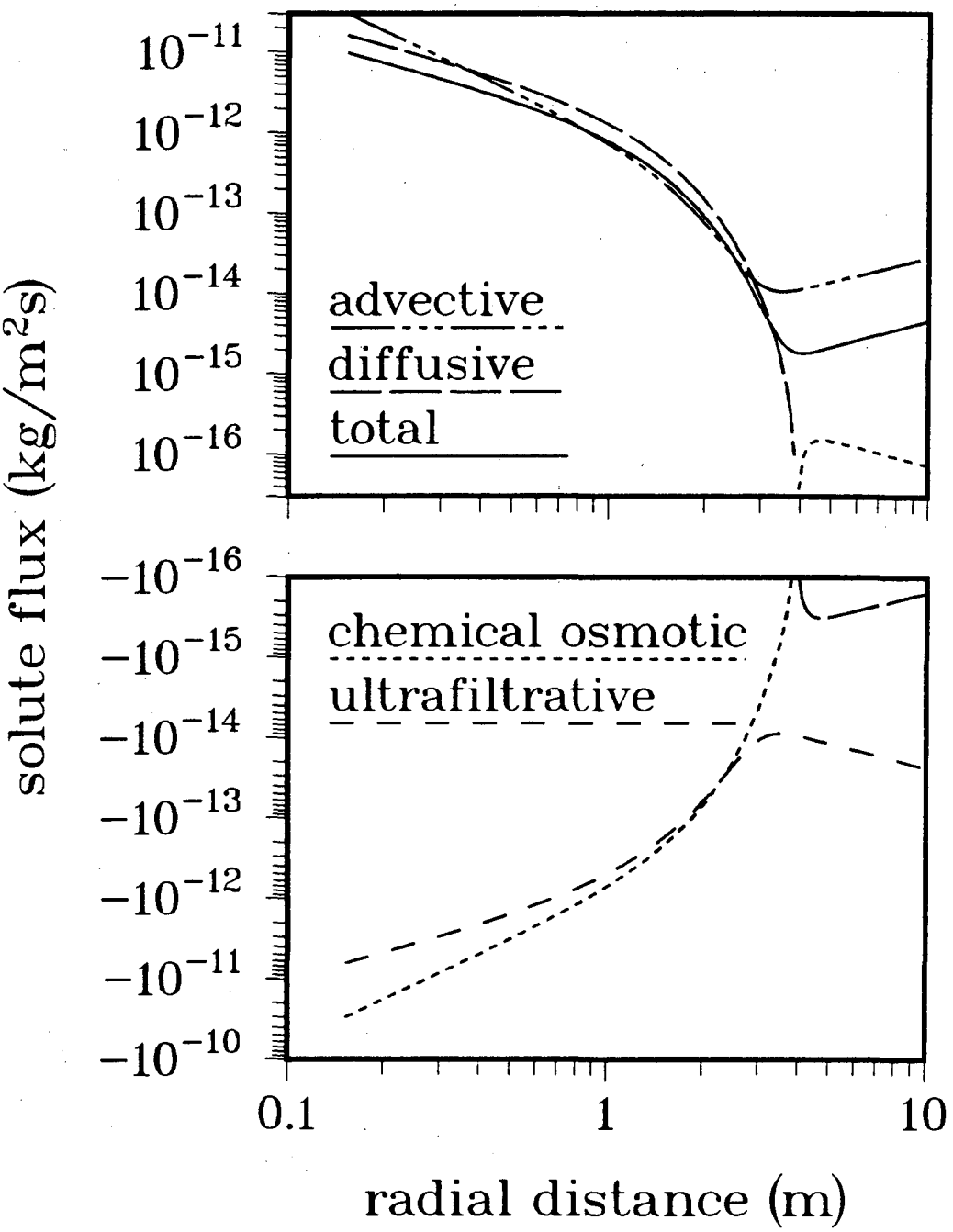

Figure 9. Individual and total solute fluxes at a simulation time of 1000 years. Chemical osmosis and ultrafiltration included. Incoming solute flux of 10^{-11} kg/m^{2}s, $L_{vs} = L_{vs} = -8 \times 10^{-17}$ kg m^2/J s.

The solute fluxes for the combined chemical osmosis and thermal osmosis case, Fig. 10, are difficult to sort out. The total flux in this case is composed of all of the fluxes named in (31). The advective and chemical osmotic fluxes are negative for all or most of the region shown. The rest of the fluxes are positive, the thermal osmotic flux being the largest individual flux. For distances greater than two meters, the absolute values of the thermal osmotic, advective and ultrafiltrative fluxes are all of the same order of magnitude, but the advective flux is negative.

An important point to note is that the incoming solute flux is constant, and therefore the total solute flux at and near the boundary must be the same for all of the cases. This is a constraint imposed by the flux boundary condition. After a distance of about one meter, the total solute flux for the uncoupled and coupled cases differ in magnitude and shape (Fig. 11). Solute migration in the chemical osmosis case is retarded relative to the uncoupled case and is the same as the uncoupled case when only thermal osmosis is considered. When both chemical osmosis and thermal osmosis are included, the solute migrates away from the flux boundary faster than in the uncoupled case and faster than when either coupled effect is considered alone.

Effects of Thermal Osmosis Only

As discussed in an earlier section, there was no difference between the temperature profiles (Fig. 3) or solute distributions (Fig. 6) for the uncoupled and thermal osmosis cases when values of $L_{qv} = L_{vq} = 3.8 \times 10^{-10}$ m^2/s were used. To obtain the results discussed in this section, the coefficients of thermal filtration and thermal osmosis were increased two orders of magnitude to 3.8×10^{-8} m^2/s. The upper limit on L_{qv} and L_{vq} based on the constraint, $L_{qq}L_{vv} - L_{qv}L_{vq} > 0$ (KATCHALSKY and CURRAN, 1967, p. 91), where $L_{qv} = L_{vq}$, is approximately 2.5×10^{-7} m^2/s, but using values larger than 3.8×10^{-8} m^2/s led to nonphysical results: the pressure near the flux boundary became negative. All of the other parameter values listed in Table 3 were kept constant, and all results are shown at a simulated time of 1000 years.

Temperature. The temperature profiles for $L_{qv} = L_{vq} = 3.8 \times 10^{-8}$ and 3.8×10^{-10} m^2/s differ very little as shown by Fig. 12. The profiles for $L_{qv} = L_{vq} = 0$ and 3.8×10^{-10} m^2/s coincide. The largest difference between the temperatures for the nonzero values of L_{qv} and L_{vq} is less than one tenth of one percent of the temperature in the uncoupled case. The finding of the previous section, that the transport of heat is unaffected by thermal filtration, is also valid for values of L_{qv} and L_{vq} between 3.8×10^{-10} and 3.8×10^{-8} m^2/s.

Pressure and Gradient of Pressure. The pressure distribution is sensitive to changes in the coefficient of thermal osmosis (Fig. 13). For values of L_{qv} and L_{vq} greater than 3.4×10^{-9} m^2/s, the change in pressure is negative for part of the range shown; for values equal to 3.8×10^{-10} m^2/s, the change in pressure is positive. For all values of L_{qv} and L_{vq}, the pressure gradient is positive and varies in magnitude as the two coefficients vary (Fig. 14). The pressure gradient corresponding to $L_{qv} = L_{vq} = 3.8 \times 10^{-8}$ m^2/s is two orders of magnitude larger than the pressure gradient for $L_{qv} = L_{vq} = 3.8 \times 10^{-10}$ m^2/s for most of the range of interest.

Solute Concentration and Solute Fluxes. The differences in the pressure gradients, and therefore advective solute fluxes, are significant suggesting that the solute distributions may also vary with the coefficient of thermal osmosis. This is not the case, however, because the thermal osmotic flux also varies with L_{vq}. The thermal osmotic flux opposes the advective flux and cancels its contribution to the total solute flux. The net result is that varying the coefficient of thermal osmosis has very little effect on the solute concentration (Fig. 15). As in the uncoupled case, near the flux boundary the total solute flux is approximately equal to the diffusive flux. After a distance of two meters, the total solute flux (not

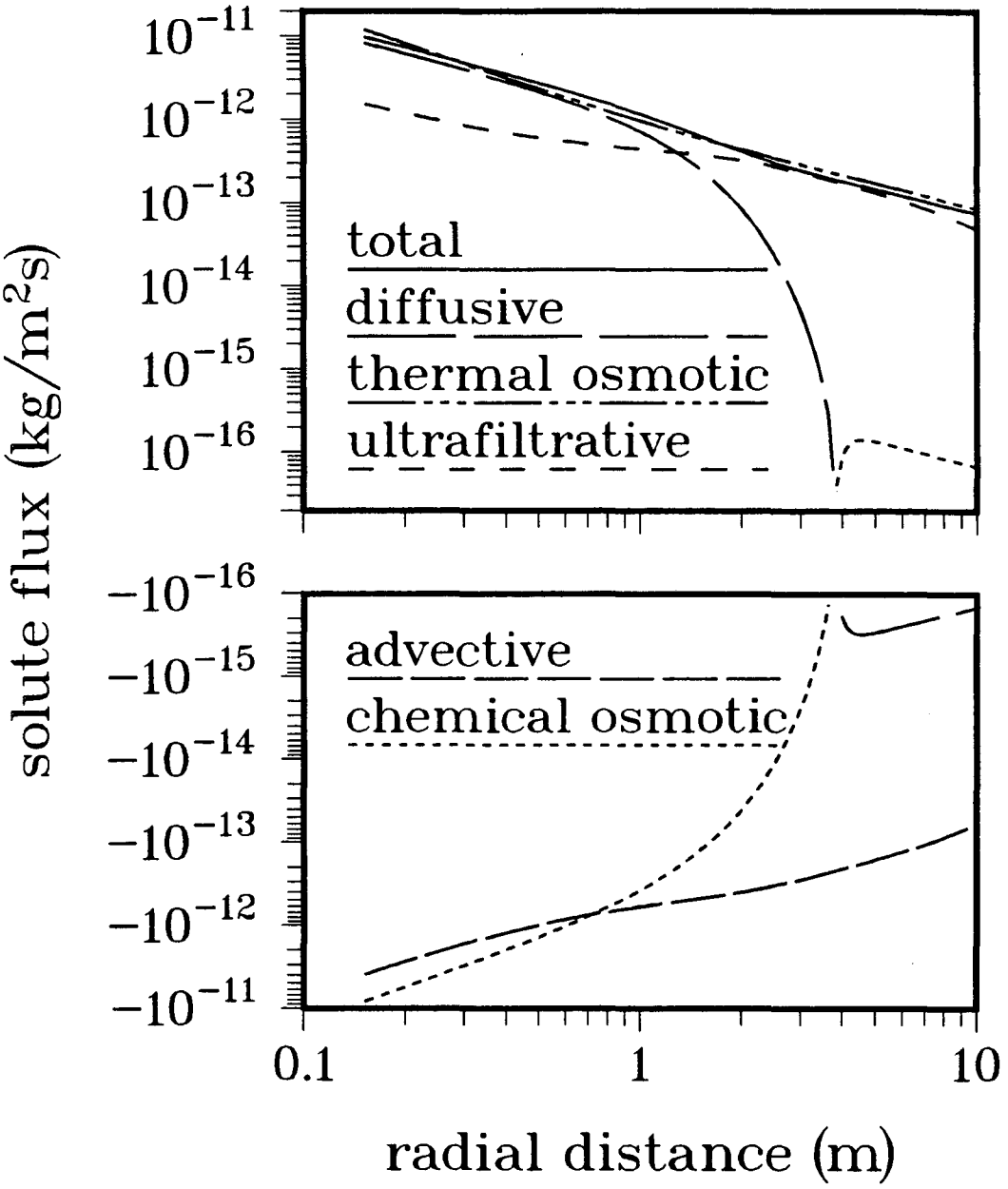

Figure 10. Individual and total solute fluxes at a simulation time of 1000 years. Thermal osmosis, thermal filtration, chemical osmosis and ultrafiltration included. Incoming solute flux of 10^{-11} kg/m^{2}s, $L_{qv} = L_{vq} = 3.8 \times 10^{-10}$ m^2/s, $L_{vs} = L_{vs} = -8 \times 10^{-17}$ kg m^2/J s.

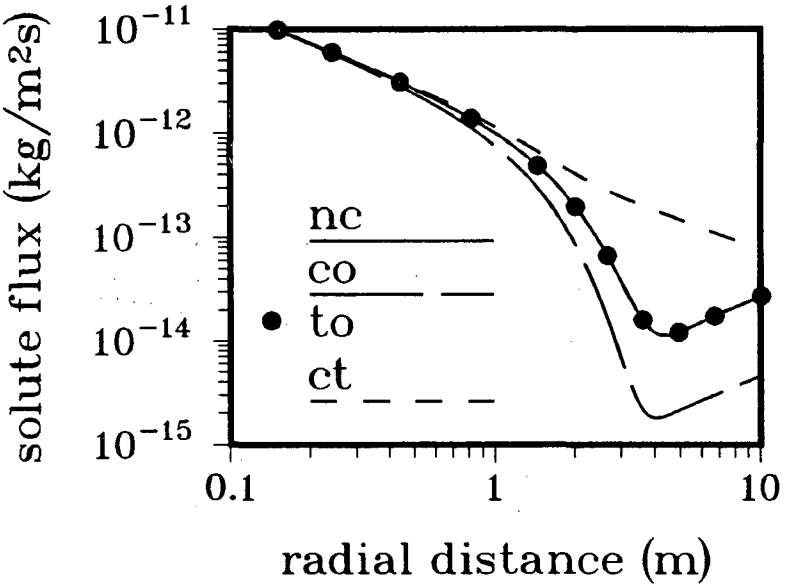

Figure 11. Total solute flux at a simulation time of 1000 years with and without coupling. Incoming solute flux of 10^{-11} kg/m^2 s, $L_{qv} = L_{vq} = 3.8 \times 10^{-10}$ m^2/s, $L_{vs} = L_{vs} = -8 \times 10^{-17}$ kg m^2/J s. **nc** – no coupling, **co** – chemical osmosis and ultrafiltration included, **to** – thermal osmosis and thermal filtration included, **ct** – all coupled processes included in **co** and **to** cases.

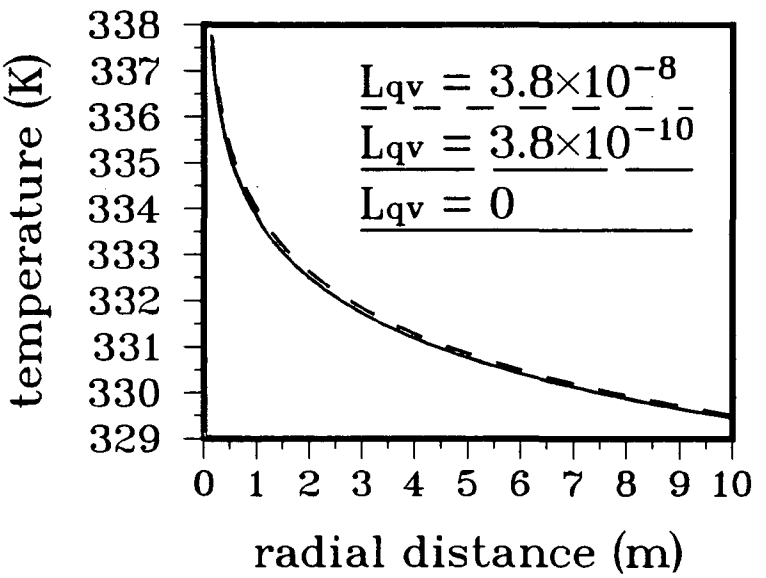

Figure 12. Temperature distribution at a simulation time of 1000 years. Thermal osmosis and thermal filtration included. Coefficients of thermal filtration (L_{qv}) and thermal osmosis (L_{vq}, $L_{vq} = L_{qv}$) varied as shown. Initial temperature of 325 K, incoming heat flux of 10 W/m^2. (Units of L_{qv} and L_{vq} are m^2/s.)

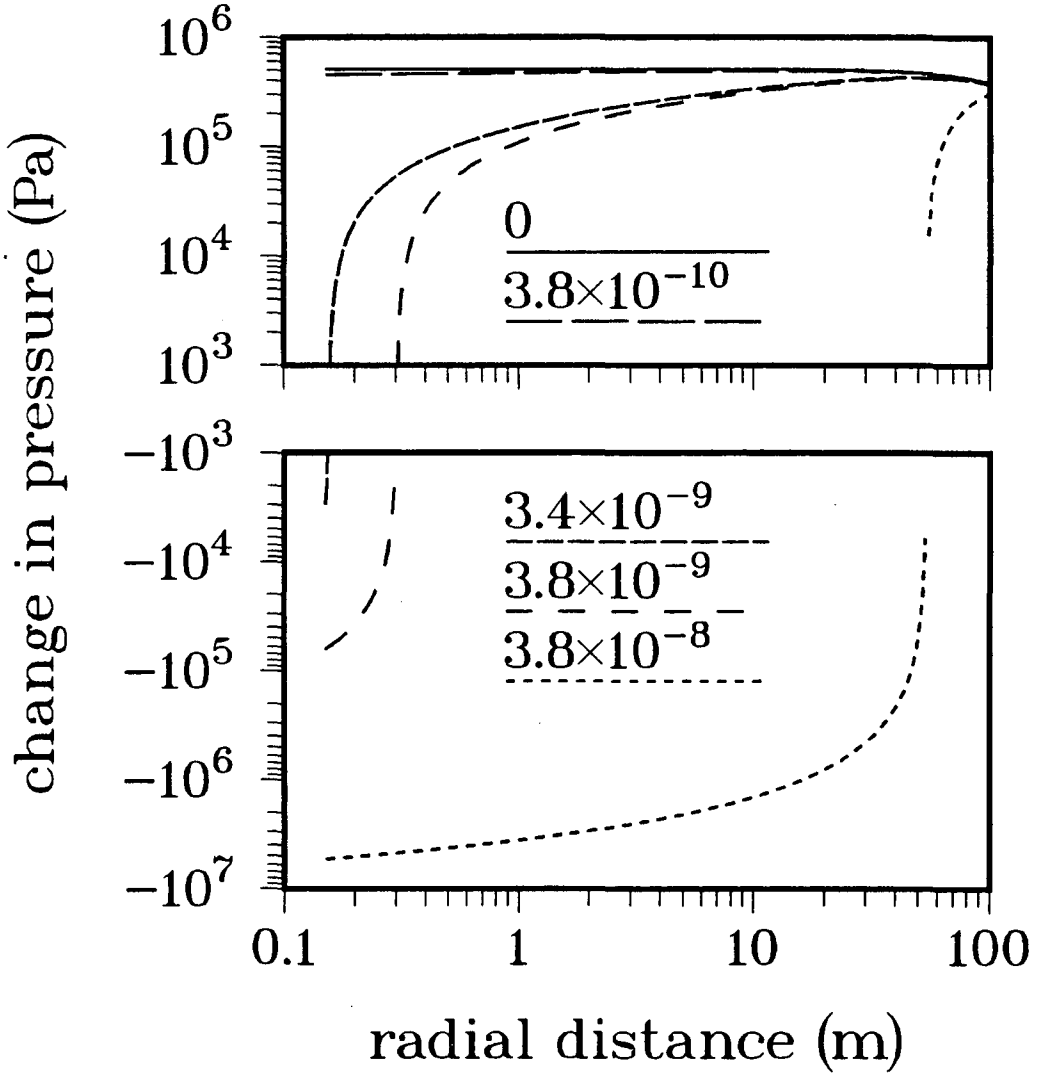

Figure 13. Change in pressure at a simulation time of 1000 years. Thermal osmosis and thermal filtration included. Coefficients of thermal filtration (L_{qv}) and thermal osmosis (L_{vq}) varied as shown. Initial pressure of 10^7 Pa. (Units of L_{qv} and L_{vq} are m^2/s.)

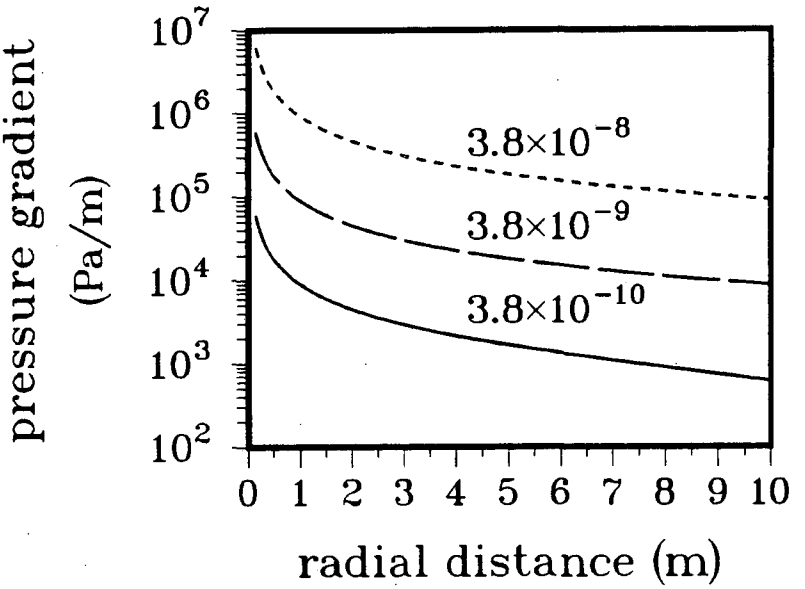

Figure 14. Pressure gradient at a simulation time of 1000 years. Thermal osmosis and thermal filtration included. Coefficients of thermal filtration (L_{qv}) and thermal osmosis (L_{vq}) varied as shown. Initial pressure of 10^7 Pa. (Units of L_{qv} and L_{vq} are m^2/s.)

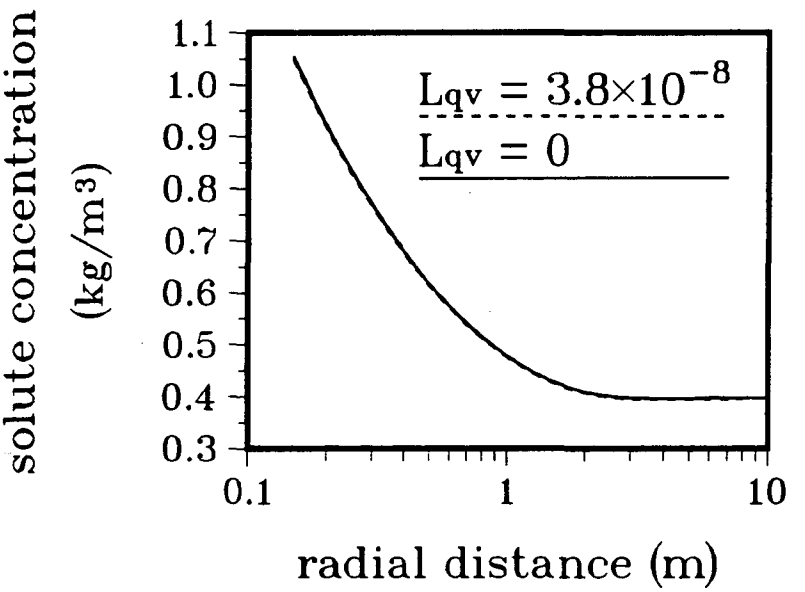

Figure 15. Solute concentration at a simulation time of 1000 years. Thermal osmosis and thermal filtration included. Coefficients of thermal filtration (L_{qv}) and thermal osmosis (L_{vq}, $L_{vq} = L_{qv}$) varied as shown. Initial solute concentration of 0.4 kg/m^3, incoming solute flux of 10^{-11} kg/m^2 s. (Units of L_{qv} and L_{vq} are m^2/s.)

plotted) equals the difference between the advective and thermal osmotic fluxes and is of the same order of magnitude for values of L_{qv} and L_{vq} between 3.8×10^{-10} and 3.8×10^{-8} m^2/s.

Effects of Chemical Osmosis Only

As discussed earlier, chemical osmosis results in pressure and solute distributions significantly different than those predicted by the uncoupled case. The temperature distributions for the two cases are identical. This section describes how the pressure and solute concentration change as L_{sv} and L_{vs}, the coefficients of ultrafiltration and chemical osmosis, are varied.

As with the previous section, all of the parameters in Table 3 were kept constant except for L_{sv} and L_{vs}, which were varied from (-8×10^{-18} to -1.2×10^{-16} kg·m^2/J·s. (When the uncoupled and chemical osmosis cases were compared earlier, a value of -8×10^{-17} kg·m^2/J·s was used.) The lower limit on L_{sv} and L_{vs} calculated from $L_{ss}L_{vv} - L_{sv}L_{vs} > 0$ (KATCHALSKY and CURRAN, 1967, p. 91), where $L_{sv} = L_{vs}$, is approximately -1.28×10^{-16} kg·m^2/J·s.

Pressure and Gradient of Pressure. The pressure profiles corresponding to different values of L_{vs} vary slightly near the flux boundary (Fig. 16). In contrast, the pressure gradients vary markedly in shape and nearly two orders of magnitude in value near the boundary (Fig. 17). The pressure gradient is negative for all values of L_{vs} between -8×10^{-18} and-1.2×10^{-16} kg·m^2/J·s and becomes more negative as L_{vs} becomes more negative. Therefore, the advective flux, which is positive, increases as L_{vs} decreases, *i.e.*, becomes more negative, and the ultrafiltrative flux becomes more negative as L_{sv} ($= L_{vs}$) decreases.

Solute Concentration and Solute Fluxes. In contrast to the thermal osmosis case, the solute concentration and fluxes for the chemical osmosis case are sensitive to small changes in L_{sv} and L_{vs} (Fig. 18). The effects of chemical osmosis and ultrafiltration act to retard the migration of solute away from the flux boundary. The more negative the values of L_{sv} and L_{vs}, the greater the retardation. As L_{sv} and L_{vs} become more negative, the total solute flux decreases and consequently, the solute concentration near the flux boundary increases. For values of L_{sv} and L_{vs} equal to -1.2×10^{-16} kg·m^2/J·s, the solute concentration at the boundary is ten times the concentration calculated for the uncoupled case. Using a value of -8×10^{-18} kg·m^2/J·s results in a concentration profile that is indistinguishable from the uncoupled case.

When L_{sv} and L_{vs} are made more negative, all of the individual solute fluxes increase in magnitude. The chemical osmotic flux and ultrafiltrative flux, both of which are negative and oppose the positive advective and diffusive fluxes, decrease resulting in a lower total solute flux away from the flux boundary. For values of the coefficients equal to -1.0×10^{-16} and -1.2×10^{-16} kg·m^2/J·s, the total solute flux is negative at radial distances greater than two meters (Fig. 19). The ultrafiltrative flux is the dominant flux at that distance. The point where the total solute flux is zero moves away from the flux boundary as the simulation time increases (Fig. 20). For times of 1, 10 and 100 years and values of L_{sv} and L_{vs} equal to -1.2×10^{-16} kg·m^2/J·s, the point of zero flux is located at 0.2, 0.3 and 0.6 meters, respectively.

SUMMARY

Governing equations that describe heat and mass transport by thermodynamically coupled processes have been solved numerically using an iterative technique, the n-dimensional Newton's method. In order to verify the computer program that implements the numerical method, results of numerical simulations were compared to analytical solutions derived for linearized approximations of the governing equations (JACOBSEN and CARNAHAN, 1990). The agreement between the analytical and numerical solutions is excellent at early simulated times when the nonlinear terms are small relative to linear terms. In addition

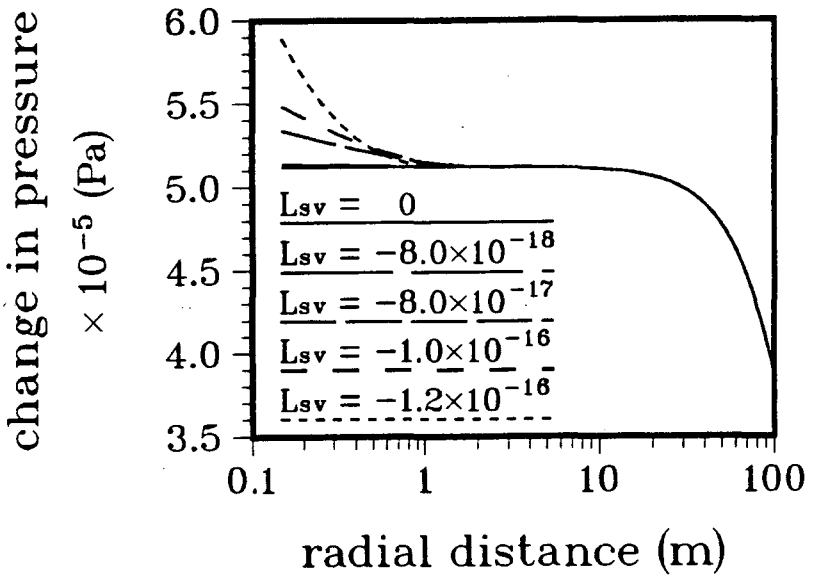

Figure 16. Change in pressure at a simulation time of 1000 years. Chemical osmosis and ultrafiltration included. Coefficients of chemical osmosis (L_{vs}) and ultrafiltration (L_{vs}, $L_{vs} = L_{vs}$) varied as shown. Initial pressure of 10^7 Pa. (Units of L_{vs} and L_{vs} are kg m^2/J s.)

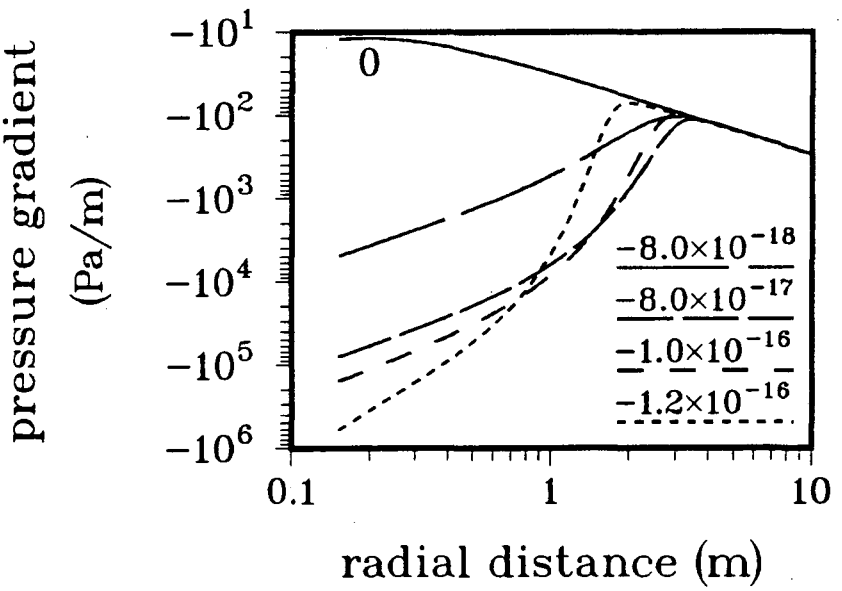

Figure 17. Pressure gradient at a simulation time of 1000 years. Chemical osmosis and ultrafiltration included. Coefficients of chemical osmosis (L_{vs}) and ultrafiltration (L_{vs}) varied as shown. Initial pressure of 10^7 Pa. (Units of L_{vs} and L_{vs} are kg m^2/J s.)

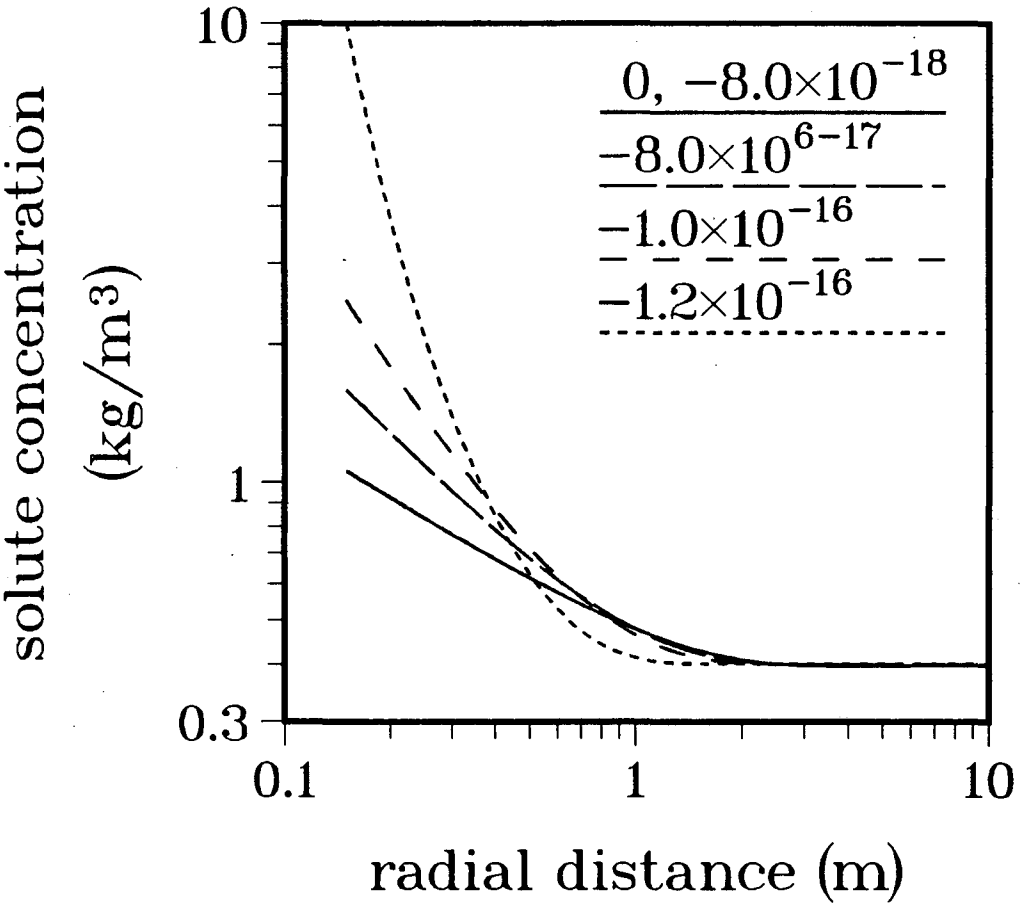

Figure 18. Solute concentration at a simulation time of 1000 years. Chemical osmosis and ultrafiltration included. Coefficients of chemical osmosis (L_{vs}) and ultrafiltration (L_{vs}) varied as shown. Initial solute concentration of 0.4 kg/m^3, incoming solute flux of 10^{-11} kg/m^2 s. (Units of L_{vs} and L_{vs} are kg m^2/J s.)

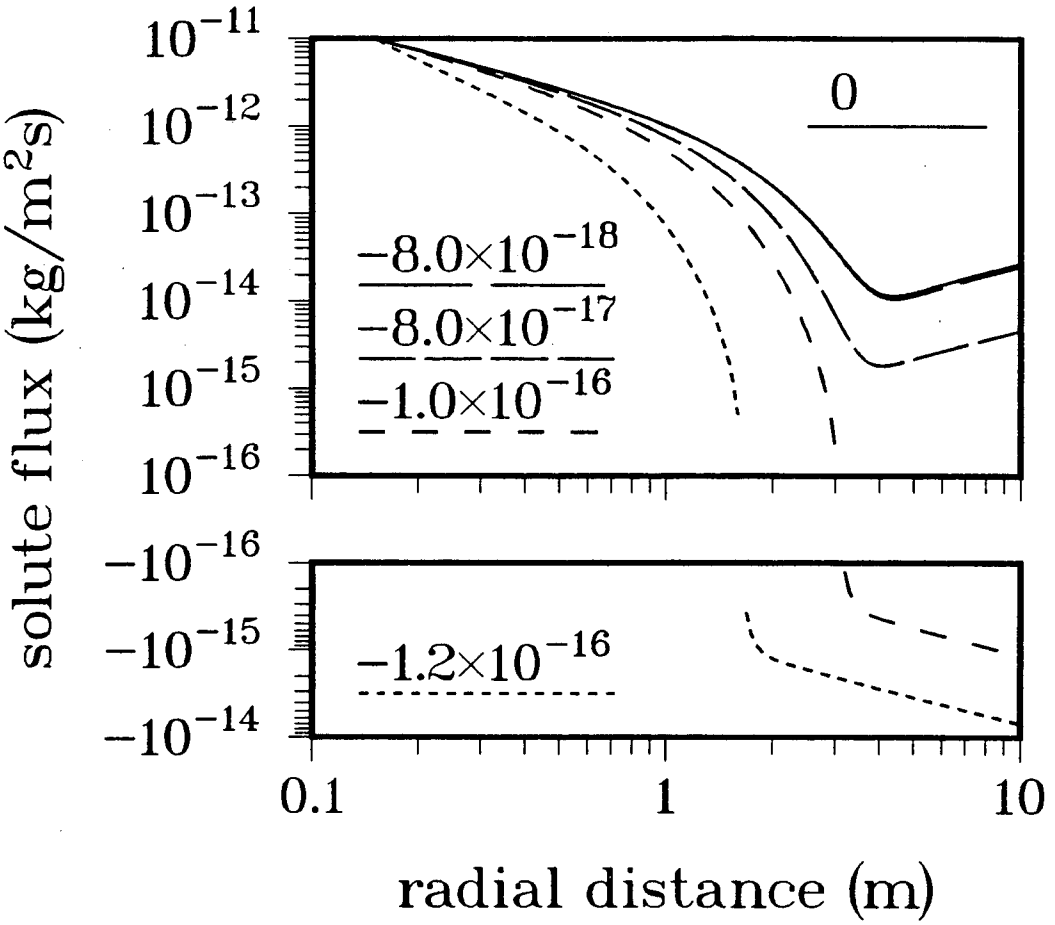

Figure 19. Total solute fluxes at a simulation time of 1000 years. Chemical osmosis and ultrafiltration included. Coefficients of chemical osmosis (L_{vs}) and ultrafiltration (L_{vs}) varied as shown. Incoming solute flux of 10^{-11} kg/m^2 s. (Units of L_{vs} and L_{vs} are kg m^2/J s.)

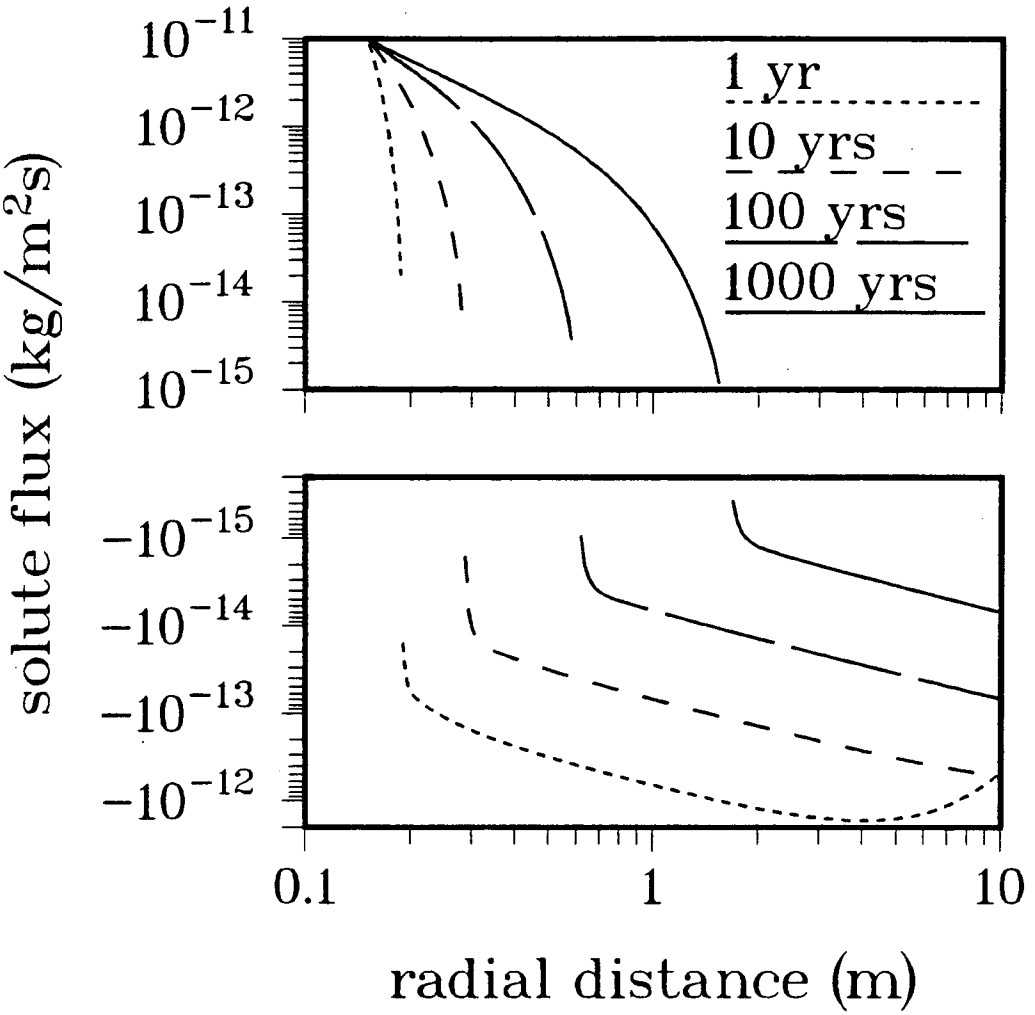

Figure 20. Total solute flux at simulation times of 1, 10, 100 and 1000 years. Chemical osmosis and ultrafiltration included. Incoming solute flux of 10^{-11} kg/m^{2}s, $L_{sv} = L_{vs} = -1.2 \times 10^{-16}$ kg m^2/J s.

to providing a check on the numerical method of solution, the analytical solutions may be used to estimate the grid size necessary to prevent undesirable boundary effects caused by using a grid too small in extent.

The computer program was used to simulate heat and mass transport in a saturated clay-like material surrounding a heat source in order to simulate transport processes that may occur in bentonite, which may be used as a packing material around a nuclear waste canister. The only coupled processes considered were chemical osmosis, ultrafiltration, thermal filtration and thermal osmosis. The results of the simulations for the parameters listed in Table 3 may be summarized as follows.

- The transport of heat by thermodynamically coupled processes is negligible compared to transport by the direct process of heat conduction. For the set of parameters used, and within a range of values of the phenomenological coefficients, the temperature calculation could be uncoupled from calculations of the pressure and solute concentration distributions.

- The pressure distribution differs for the uncoupled and coupled cases. The differences are largest near the flux boundary and decrease with distance from it. The resulting differences in the pressure gradient for the uncoupled and coupled cases lead to differences in the advective flux for each case. When chemical osmosis and ultrafiltration are included in the simulation, the advective flux is cancelled by the chemical osmotic flux at the flux boundary. When thermal osmosis and thermal filtration are included, the advective flux is cancelled by the thermal osmotic flux. Finally, when all of these coupled processes are included, the advective flux is cancelled by the sum of the chemical osmotic and thermal osmotic fluxes. The result is that the total solute flux near the flux boundary is dominated by the diffusive flux in all cases. The only variance from this is that when chemical osmosis and therefore also ultrafiltration are included, the diffusive flux is opposed, but not cancelled, by the ultrafiltrative flux.

- The solute concentration profiles for the uncoupled and thermal osmosis cases are nearly identical for most values of L_{qv} and L_{vq} used. The differences in the profiles increase as L_{qv} and L_{vq} increase. When only chemical osmosis is included, the solute concentration near the flux boundary is larger than the concentration for the uncoupled case, and as L_{sv} and L_{vs} become more negative, the magnitude of the difference increases. When both chemical osmosis and thermal osmosis are included, the solute concentration is smaller than that of the uncoupled case.

- The total solute flux at the inner boundary has been constrained by the flux boundary condition imposed there, but differences in the total solute flux for the uncoupled and coupled cases do occur at short distances from the boundary. When chemical osmosis is included, the total solute flux is retarded relative to the uncoupled case. The total solute flux for the thermal osmosis case is the same as that for the uncoupled case. When both chemical osmosis and thermal osmosis are included, the solute migration away from the flux boundary is faster than that of the uncoupled case.

The last point above is particularly important in trying to understand and simulate transport processes in the vicinity of a nuclear waste canister. Based on the solute profiles for the thermal osmosis case (Figs. 6 and 15) and the chemical osmosis case (Figs. 6 and 18), one might conclude that thermal osmosis does not affect solute migration and that the only significant coupled process is chemical osmosis, which retards the solute migration away from the flux boundary. Figure 11, which is a plot of the total solute flux for the uncoupled and all coupled cases, shows that these conclusions are erroneous: when both chemical osmosis and thermal osmosis are included, the rate of solute migration away from the flux boundary is accelerated relative to the uncoupled case. Because it depends on the material properties, phenomenological coefficients, and input heat and solute fluxes used, this result, as well as those stated

earlier, cannot be generalized. Nevertheless, these results demonstrate the importance of including thermodynamically coupled processes when simulating transport through a clay-like medium.

The numerical simulator described in this work may be used to investigate heat and mass transport through other geologic media possessing the properties of a semipermeable membrane. Examples of such applications are water movement in irrigated soils with high salt contents and contaminant transport in clay formations. Crucial to understanding transport processes in these cases is the realization that because of the properties of the environment in which transport is taking place, processes other than the direct processes of advection, diffusion and heat conduction may contribute significantly to heat and mass flows.

Acknowledgements. — This work was supported by the Director, Office of Energy Research, Office of Basic Energy Sciences, Engineering and Geosciences Division, of the U. S. Department of Energy under Contract No. DE–AC03–76SF00098. The authors would like to thank Karsten Pruess for his careful review of the manuscript and his thoughtful comments and suggestions.

REFERENCES

ABRIOLA L. M. and PINDER G. F. (1985) A multiphase approach to the modeling of porous media contamination by organic compounds. 2: Numerical simulation. *Water Resour. Res.* **21**, 19–26.

CARNAHAN C. L. (1987) Simulation of uranium transport with variable temperature and oxidation potential: The computer program THCC. In *Scientific Basis for Nuclear Waste Management IX* (eds. J. K. BATES and W. B. SEEFELDT), pp. 713–721. Materials Research Society.

CARNAHAN C. L. and JACOBSEN J. S. (1990) Coupled Transport Processes in Semipermeable Media. Part I: Theoretical Basis. *Lawrence Berkeley Laboratory Report LBL–25618.*

CRANK J. (1975) *The Mathematics of Diffusion* (2nd ed.). Clarendon Press. 414p.

CUYT A. A. M. and RALL L. B. (1985) Computational implementation of the multivariate Halley method for solving nonlinear systems of equations. *ACM Trans. Math. Softw.* **11**, 20–36.

DAHLQUIST G. and BJÖRCK A. (1974). *Numerical Methods.* Prentice-Hall. 573p.

HINDMARSH A. C. (1977) Solution of Block-Tridiagonal Systems of Linear Equations. *Lawrence Livermore National Laboratory Report UCID-30150.*

ISAACSON E. and KELLER H. B. (1966) *Analysis of Numerical Methods.* John Wiley & Sons. 541p.

JACOBSEN J. S. and CARNAHAN C. L. (1990) Coupled Transport Processes in Semipermeable Media: Analytical Solutions of the Linearized Governing Equations. *Lawrence Berkeley Laboratory Report LBL–24725.*

KELL G. S. (1972) Thermodynamic and transport properties of fluid water. In *Water, A Comprehensive Treatise: Volume 1, The Physics and Physical Chemistry of Water* (ed. F. FRANKS), Chap. 10, pp. 363–412. Plenum Press.

LETEY J. and KEMPER W. D. (1969) Movement of water and salt through a clay-water system: Experimental verification of Onsager reciprocal relation. *Soil Sci. Soc. Amer. Proc.* **33**, 25–29.

MILLER C. W. and L. V. BENSON (1983) Simulation of solute transport in a chemically reactive heterogeneous system: Model development and application. *Water Resour. Res.* **19**, 381–391.

MOSS M. and MOLECKE M. A. (1983) Thermal conductivity of bentonite/quartz high-level waste package backfill. In *Scientific Basis for Nuclear Waste Management VI* (ed. D. G. BROOKINS), pp. 719–726. Elsevier Science Publishing Co.

ORTEGA J. M. and RHEINBOLDT W. C. (1970) *Iterative Solution of Non-Linear Equations in Several Variables.* Academic Press. 572p.

PITZER K. S., PEIPER J. C. and BUSEY R. H. (1984) Thermodynamic properties of aqueous sodium chloride solutions. *J. Phys. Chem. Ref. Data* **13**, 1–89.

ROGERS, P. S. Z. and PITZER K. S. (1982) Volumetric properties of aqueous sodium chloride. *J. Phys. Chem. Ref. Data* **11**, 15–81.

STEHFEST H. (1970) Algorithm 368: Numerical inversion of Laplace transforms. *ACM Comm.* **3**, 47–49.

SRIVASTAVA R. C. and AVASTHI P. K. (1975) Non-equilibrium thermodynamics of thermo-osmosis of water through kaolinite. *J. Hydrol.* **24**, 111–120.

APPENDIX: IMPLEMENTATION OF THE CONSTANT-FLUX CONDITION

Implementation of the constant-flux condition at the inner boundary is difficult because of the coupling of temperature, pressure and solute concentration in the phenomenological equations (7, 8, 9). Given constant incoming heat ($J_{q,inc}$), solute ($J_{s,inc}$) and solvent ($J_{0,inc}$) fluxes, the incoming volume flux ($J_{v,inc}$) is calculated from

$$J_{v,inc} = \overline{V}_0 J_{0,inc} + \overline{V}_s J_{s,inc}, \tag{A-1}$$

and J_s° at the flux boundary is calculated from (11), rewritten as

$$J^\circ_{s,inc} = \frac{J_{s,inc} - C_s J_{v,inc}}{1 - C_s \overline{V}_s}. \tag{A-2}$$

The values of $J_{q,inc}$, $J_{v,inc}$ and $J^\circ_{s,inc}$ are substituted into the phenomenological equations (7, 8, 9), and the partial derivatives are replaced by finite difference approximations centered at node 1 (CRANK, 1975, p. 147). For example, in the case of an even grid spacing of Δx,

$$\left(\frac{\partial P}{\partial x}\right)_{\text{node 1}} \approx \frac{P_2 - P_0}{2\Delta x}, \tag{A-3}$$

where P_i is the pressure at node i. The subscript 0 in the equation above refers to an imaginary node, that is, the variable values at node 0 are never explicitly calculated. The equations for $J_{q,inc}$, $J_{v,inc}$ and $J^\circ_{s,inc}$ are solved for the temperature, pressure and solute concentration at node 0, and the results are substituted into the governing equations in which the finite difference approximations replacing the space derivatives are centered at node 1 and therefore, involve the variable values at nodes 0, 1 and 2. Rearranging the governing equations after the substitution yields residue equations for temperature, pressure and solute concentration at node 1. These equations involve variable values at only nodes 1 and 2, but are second order correct in Δx.

LAWRENCE BERKELEY LABORATORY
UNIVERSITY OF CALIFORNIA
INFORMATION RESOURCES DEPARTMENT
BERKELEY, CALIFORNIA 94720